hv photonics

IMPACT FACTOR 2.1

CITESCORE 2.6

Review

Acceleration of Heavy Ions by Ultrafast High-Peak-Power Lasers: Advances, Challenges, and Perspectives

Jan Badziak and Jarosław Domański

Special Issue

Advances in Ultrafast Laser Science and Applications

Edited by

Dr. Shuai Yuan, Dr. Mengyun Hu, Dr. Min Li and Dr. Cang Jin

MDPI

https://doi.org/10.3390/photonics12030184

photonics

MDPI

Review

Acceleration of Heavy Ions by Ultrafast High-Peak-Power Lasers: Advances, Challenges, and Perspectives

Jan Badziak * and Jarosław Domański

Institute of Plasma Physics and Laser Microfusion, 01-497 Warsaw, Poland
* Correspondence: jan.badziak@ifpilm.pl

Abstract: Laser-driven ion acceleration is a new, rapidly developing field of research and one of the important applications of ultrafast high-peak-power lasers. In this acceleration method, extremely strong electric fields, induced by an ultrafast laser in the plasma generated by the laser–target interaction, enable the acceleration of ions to relativistic velocities on picosecond time scales and at sub-millimetre distances. This opens the prospect of constructing a fundamentally new type of high-energy ion accelerator—less complex, more compact, and cheaper than the ion accelerators operating today. This paper briefly discusses the basic mechanisms of heavy ion acceleration driven by an ultrafast high-peak-power laser and summarises the advances in experimental and numerical studies of laser-driven heavy ion acceleration. The main challenges facing this research and the prospects for the application of laser-accelerated heavy ion beams are outlined.

Keywords: laser-driven ion accelerators; heavy ions; ultrafast lasers; high-peak-power lasers; laser–plasma interaction

check for updates

Received: 18 January 2025
Revised: 19 February 2025
Accepted: 20 February 2025
Published: 23 February 2025

Citation: Badziak, J.; Domański, J. Acceleration of Heavy Ions by Ultrafast High-Peak-Power Lasers: Advances, Challenges, and Perspectives. *Photonics* **2025**, *12*, 184. https://doi.org/10.3390/photonics12030184

Copyright: © 2025 by the authors. Licensee MDPI, Basel, Switzerland. This article is an open access article distributed under the terms and conditions of the Creative Commons Attribution (CC BY) license (https://creativecommons.org/licenses/by/4.0/).

1. Introduction

High-energy heavy ion beams are widely used in nuclear and particle physics. Studies of collisions of heavy ions with very high energies (hundreds of GeV and higher) allow us to understand the structure of matter at its most elementary level, to study the nature of the forces that bind quarks in hadrons or the structure of particles such as protons and neutrons. They also allow us to look back into the past, to the times before the creation of hadrons, and to study the early evolution of the universe. Heavy ion beams are also increasingly used in other fields of research, such as high energy-density physics (HEDPs), inertial confinement fusion (ICF) or materials science. The basic source of high-energy heavy ions are conventional RF-driven accelerators. Due to the relatively low strengths of the accelerating fields in these accelerators (below ~1 MV/cm), acceleration of ions to high energies requires very long acceleration paths, which, combined with other limitations in the design of these accelerators, causes RF-driven accelerators to be very large (up to hundreds of meters in size), complex, and expensive devices.

One of the potential alternatives, or at least a significant supplement to conventional ion accelerators, are ion accelerators driven by a laser (e.g., [1–4]). The main components of this accelerator are a high-peak-power laser and a target (solid, liquid or gas) placed in a vacuum chamber. When the laser beam intensity is high enough, the interaction of the beam with the target leads to the creation of plasma, i.e., a state of matter comprising free electrons and ions. As a result of the action of the laser field on electrons and ions in the plasma, due to the significant difference in the masses of these particles, a separation of some (usually most) electrons from ions occurs. Between the layer of the electrons and the

ions, a very strong quasi-static electric field is created which pulls the ions following the moving electron layer accelerated by the laser field force. The strength of this quasi-static electric field depends on the intensity of the laser beam and can reach values from GV/cm to TV/cm, i.e., values many orders of magnitude higher than those achieved by accelerating fields in conventional accelerators. As a result, ions can be accelerated to high energies over sub-mm distances and in picosecond time periods, i.e., over distances and time periods at least several orders of magnitude shorter than in the case of conventional accelerators (for details see Section 2). Thus, the laser-driven accelerator can be a much smaller, less complex, and much cheaper device than the conventional one.

In addition to smaller dimensions, future laser-driven accelerators may have a number of other properties unavailable to conventional accelerators. The most important of them include many orders of magnitude higher ion beam densities, fluences and intensities and very short ion pulse durations (down to picoseconds or even femtoseconds) (e.g., [4,5]). In the light of current knowledge, it can be assumed that a significant disadvantage of laser-driven accelerators in comparison to RF-driven ones will be a wider energy spectrum of the produced ion beams, lower energy efficiency of the accelerator as a whole (taking into account the energy efficiency of the laser driver) and a lower accelerator repetition rate. It is also possible to suppose that achieving multi-TeV ion energies, currently available in the largest conventional accelerators (e.g., in the LHC accelerator at CERN), will be extremely difficult in the case of laser accelerators.

The above-mentioned features of laser-driven accelerators apply to both light ions (protons, Li ions, C ions, etc.) and heavy ions (Cu, Ag, Au, Pb ions, etc.). However, the requirements for the laser driver ensuring that the ion beam achieves practically useful parameters are usually different for light and heavy ions, and concern primarily the intensity and energy of the laser beam driving ions. In the case of light ions, laser intensities (I_L) below 10^{12} W/cm^2 and sub-joule laser energies (E_L), easily achievable by commercially available long-pulse (nano- or sub-nanosecond) lasers, enable obtaining light ion energies of the order of multi-keV/u, which can be useful in some applications. These low requirements meant that the first effects of ion acceleration in laser-generated plasma were observed already in the sixties of the last century [6]. With the increasing ion mass (atomic mass number A of the ion), the requirements for laser beam intensity and energy increase. For example, the effective acceleration of ions with A ~ 100–200 to energy ~ multi-keV/u usually requires an intensity of ~10^{13}–10^{14} W/cm^2 and an energy (E_L) of ~1 J of a long laser pulse, while the production of heavy, multi-charged multi-MeV ions requires I_L ~ 10^{15}–10^{16} W/cm^2 and E_L ~ 100 J or higher (e.g., [7]). In the case of ultrafast lasers, i.e., lasers generating pico- or femtosecond pulses, obtaining ion energies similar to those achieved with a long-pulse laser requires higher laser intensities but is usually possible at much lower laser energies (see Sections 2 and 3).

Long-pulse lasers with parameters enabling heavy ion acceleration to multi-MeV energies were already available in the 1980s, but intensive development of research on heavy ion acceleration using such lasers took place mainly in the years 1990–2010. A summary of the most important results from that period can be found, for example, in [7–9]. However, heavy ion beams generated by long-pulse lasers have a number of disadvantages that make their practical use difficult. These include, in particular, a wide quasi-Maxwellian energy spectrum, large angular divergence, rather inhomogeneous spatial structure and a complex and poorly controllable ionisation spectrum containing a large number of ion charge states. Moreover, due to the long-pulse duration and relatively large focal spot of the laser beam (typically, of the order of 100 μm), achieving laser intensities of ~10^{15}–10^{16} W/cm^2 requires high laser energies in the sub-kilojoule range or higher. At the current level of laser technology, laser systems providing such energies can operate with a very

low repetition rate (usually no more than one shot every few minutes), which greatly limits the range of possible applications of ion beams generated by such lasers.

Considering the limitations of long-pulse lasers (in particular, the limitation of the maximum achievable laser intensity to about 10^{17} W/cm^2) as well as the disadvantages of ion beams produced using these lasers, a real breakthrough in research on laser-driven ion acceleration was the use—at the turn of the last and present century—of high-peak-power ultrafast lasers for these researches (see e.g., [1–4] and the references therein). These lasers have the ability to achieve laser intensities several orders of magnitude higher than achievable in long-pulse lasers at comparable laser pulse energies. They make it possible to achieve not only much higher ion energies, but also to produce ion beams with much better quality than in the case of using a long-pulse laser as an ion driver.

In the last two decades, the development of ultrafast high-peak-power laser technology has been impressive and has resulted in the growth of the energy of these lasers from sub-J to over 100 J, peak power from multi-TW to several PW [10,11], and laser intensity from 10^{18}–10^{19} W/cm^2 to 10^{22}–10^{23} W/cm^2 [12,13]. This has allowed the increase in the energy of laser-driven heavy ions from the multi-MeV range to the GeV range (see Section 3). The increase in the peak power of the laser pulse to the level of ~100 PW and laser intensity to ~10^{24} W/cm^2, expected in the currently designed ultrafast lasers [10,14–16], would open the way to the production of heavy ions with energies in the sub-TeV and perhaps TeV range, i.e., with energies comparable to those achieved in the largest conventional heavy ion accelerators currently in operation. Achieving such ion energies in a high-quality laser-generated ion beam, combined with the other unique features of this beam mentioned earlier, would open up the prospect of exploring new research areas in nuclear physics and HEDP, and perhaps in other fields as well.

This paper briefly discusses basic mechanisms of laser-driven ion acceleration and summarises the advances in research on heavy ion acceleration driven by ultrafast high-peak-power lasers. Also, it outlines the main challenges facing this research and some potential applications of heavy ion beams produced in laser-driven accelerators. In Section 2, the basic mechanisms of laser-driven ion acceleration, including the mechanisms dominating heavy ion acceleration, are discussed. Section 3 briefly summarises the most important results of laser-driven heavy ion acceleration studies conducted in the last two decades at moderate (below 10^{19} W/cm^2) and high (up to 10^{22} W/cm^2) ultrafast laser beam intensities. Section 4 presents selected results of numerical studies of heavy ion acceleration at ultra-high intensities of ~10^{23} W/cm^2 expected to be achieved in currently operating and emerging multi-PW lasers. Section 5 outlines the main challenges facing research on laser-driven heavy ion acceleration, while Section 6 highlights the prospects for some applications of laser-accelerated heavy ion beams.

2. Basic Mechanisms of Laser-Driven Acceleration of Ions

As mentioned in Introduction, the interaction of an intense laser beam with a target (solid, liquid or gas) results in the creation of a plasma, i.e., a medium composed of electrons and ions. In this plasma, electromagnetic (EM) and hydrodynamic (thermal) forces are induced, which stimulate the movement of electrons and ions.

In the case of relatively low laser intensities (~10^{10}–10^{15} W/cm^2) and long laser pulses (from tens of ps to tens of ns), the vast majority of plasma ions are accelerated by hydrodynamic forces (thermal pressure of the plasma medium). The ion velocity is relatively small (~10^6–10^8 cm/s), but the number of accelerated ions in the case of dense targets (solid or liquid) can be very large. As a result, the energies of generated ion streams (actually plasma streams, as ions move together with the electron cloud) can constitute from several to several dozen percent of the laser energy. Such ion/plasma streams ablating from

the target surface towards the laser (backwards) can, in particular, accelerate the remaining part of the target in the forward direction (due to the recoil force) and play a fundamental role in hydrodynamic macroparticle accelerators [17–22], and in inertial nuclear fusion where they are used to accelerate and compress fusion targets containing nuclear fuel (DT or other) [23–25]. It should be added, however, that in the plasma generated by long laser pulses, in which the motion of the bulk of ions is determined by hydrodynamic forces, there are also strong EM fields that can accelerate ions to speeds much higher than those achieved due to the hydrodynamic motion. These fields arise as a result of the non-uniform distribution of electron density and temperature in the plasma and can produce "supra-thermal" (fast) ions with multi-MeV energies [7–9]. The number of these ions is usually 2–3 orders of magnitude smaller than the number of "thermal" ions accelerated by hydrodynamic forces and, as a result, the total energy of the fast ion stream is usually a small fraction of the energy of the "thermal" ion stream.

In the case of laser intensities $>10^{16}$ W/cm^2, the motion of electrons and ions in the laser-generated plasma is determined by EM forces. At laser intensities $>10^{18}$ W/cm^2, the electrons are accelerated by these forces to speeds close to the speed of light c; hence, such intensities are usually called relativistic intensities. The strength of electric fields induced in plasma at relativistic laser intensities can reach enormous values (from GV/cm to TV/cm) and, as a result, these fields can accelerate ions to high velocities v_i, including relativistic ones ($v_i \approx c$), over sub-mm distances. Relativistic laser intensities are now commonly produced by focused beams of high-power ultrafast lasers generating femto- and picosecond pulses, and experimentally demonstrated laser intensities reach 10^{23} W/cm^2 [13]. It is predicted that in currently constructed or designed multi-PW ultrafast lasers, the power of the femtosecond laser pulse will reach 10–100 PW, and the laser intensity in the focused beam will be close to 10^{24}–10^{25} W/cm^2 [10,14–16]. At such laser intensities, it seems possible to accelerate ions to energies of ~TeV, comparable to the energies of ions produced in the largest conventional RF-driven accelerators.

At relativistic laser intensities, the main source of EM forces accelerating ions in the plasma is the Lorenz force $\mathbf{F} = q\,\mathbf{E} + q\,(\mathbf{v} \times \mathbf{B})$, where q is the charge of the accelerated particle, v is the particle velocity, and **E** and **B** are the electric and magnetic parts of the laser field in the plasma. This force interacts with both plasma electrons and plasma ions. However, due to the large mass of the ion, at laser intensities $<10^{24}$ W/cm^2, the motion of ions due to the direct action of the Lorenz force can usually be neglected and, in practice, only electrons are set in motion by this force. The electrons are pushed away from the ions (from the equilibrium position) by the force, which results in creating a very strong electric field between the ions and the moving electron cloud. This electric field accelerates the ions, which usually move together with the electron cloud. Since the electric field strength is extremely high, ions can reach high velocities and energies over very short distances (from tens to hundreds of micrometres) and in very short periods of time (from tens of fs to several ps). The detailed mechanism of ion acceleration is determined by the physical conditions of laser–target interaction and depends on both the laser pulse parameters and the target parameters. In the last more than twenty years of research on ion acceleration driven by a short laser pulse of relativistic intensity, several effective acceleration mechanisms have been proposed and investigated. These include target normal shield acceleration (TNSA) [1–4,26–35], radiation pressure acceleration (RPA) [1–4,36–45], skin layer ponderomotive acceleration (SLPA) [7,46–48], collisionless electrostatic shock acceleration (CESA) [1–4,49,50], Coulomb explosion acceleration (CEA) [1–4,51–55], laser afterburner acceleration (BOA, sometimes called relativistic induced transparency acceleration—RITA) [1–4,56–59], magnetic vortex acceleration (MVA) [60,61], and solitary ion wave acceleration (ISWA) [62,63]. The actual ion acceleration process usually includes two

or more of the mechanisms indicated above and the final parameters of the generated ion beam are the result of the contribution of each of the mechanisms participating in this process.

The acceleration mechanisms listed above basically enable the acceleration of ions with very different atomic mass numbers, A, starting from protons and ending with super-heavy ions with mass numbers A $\geq$ 200. The effectiveness of the mechanism strongly depends on the mass of the accelerated ion and the laser parameters, in particular, the laser intensity and the energy fluence of the laser beam. Particularly large differences, both in terms of the effectiveness of the individual acceleration mechanisms listed above and the required laser parameters, occur between the acceleration of protons and light ions and the acceleration of heavy ions, by which we will understand here ions with mass numbers A >> 10 (e.g., A > 50). The main reasons for these differences are as follows: (1) Heavy ions are usually not fully ionised and the ion beam contains multiple ion species with different charge states Z which are simultaneously accelerated by electric fields induced in the plasma. (2) The ratio of the charge q to the mass m of the ion s = q/m = Z/A is much lower than for protons or light ions, which significantly reduces the ion acceleration efficiency. (3) Efficient acceleration of heavy ions to high speeds (sub-relativistic or relativistic) is only possible at very high laser intensities (I_L ~ 10^{22}–10^{23} W/cm^2 or higher); at such high intensities the average charge state Z_{mean} of the ions in the beam is high (Z_{mean} >> 10), which causes the Coulomb explosion of the ions in the beam to have a significant effect on the ion acceleration process. (4) Because Z_{mean} >> 10, the electron density of the plasma in which the ions are accelerated is much higher than in the case of light ions or protons, which affects the plasma properties. (5) The large masses and energies of heavy ions cause the influence of the electromagnetic field occurring in the acceleration zone and outside this zone on the ion motion to be smaller than in the case of light ions and protons. The above differences between the acceleration of heavy and light ions increase with the increase in the ion mass and are particularly evident in the case of acceleration of super-heavy ions.

Recent studies on laser-driven heavy ion acceleration have shown [5,64,65] that to achieve high heavy ion energies (multi-GeV and higher) desired in numerous applications of heavy ion beams (e.g., in nuclear physics, high energy-density physics or inertial confinement nuclear fusion), very high laser intensities (so-called ultra-relativistic or ultra-high intensities) reaching values of ~10^{23} W/cm^2 or even higher are necessary. Such high intensities are also desirable due to the need to obtain high charge states Z of the ion (due to field ionisation of the atom/ion) and thus a high value of the Z/A ratio necessary for achieving high acceleration efficiency [64,65]. At ultra-relativistic laser intensities, the dominant mechanism of heavy ion acceleration is usually the RPA mechanism [5,64–66]. This mechanism is a fundamental factor enabling the transformation of laser energy into ion energy and to the greatest extent determines the energy of the vast majority of ions in the generated ion beam. However, the RPA mechanism ends with the termination of the laser pulse irradiating the ion target. After the termination of the laser pulse, the acceleration process is continued by the TNSA mechanism, in which the source of the electric field accelerating the ions is the sheath of high-energy (supra-thermal) electrons produced in laser–plasma interactions. Additionally, since the Coulomb forces acting between highly ionised heavy ions are not fully compensated by the cloud of electrons surrounding the ions, the ions are accelerated by the CEA mechanism. The CEA mechanism becomes important when the ionisation level Z of ions is sufficiently high, which usually occurs already in the initial stage of laser–target interaction. This mechanism therefore operates both in the RPA and TNSA acceleration stages. Moreover, if the laser pulse of relativistic intensity is sufficiently long (or the target is sufficiently thin), the RPA acceleration stage can be followed by ion acceleration in the RITA regime. Thus, various acceleration mechanisms can participate in the heavy ion

acceleration process and their contribution to and importance in this process depend on the laser and target parameters. For the set of parameters that are achievable currently or in the near future and that potentially enable achieving heavy ion beam parameters useful for applications, the most important of these mechanisms can be considered RPA and TNSA. Below, these mechanisms are described in detail. The basic properties of the CEA mechanism are also outlined.

2.1. Ion Acceleration by the Radiation Pressure Acceleration (RPA) Mechanism

When a short (fs or ps) laser pulse of relativistic intensity irradiates a dense target, the low-intensity part of the pulse's leading edge is usually intense enough to ionise the target surface and generate a plasma (pre-plasma) on it. The main part of the pulse carrying the vast majority of the laser energy interacts with the pre-plasma and in the skin layer near the surface where the plasma electron density, n_e, reaches the so-called critical density, n_{ec}, and induces two oppositely directed ponderomotive forces F_p (Figure 1). Each of these forces acts on the plasma electrons located in the skin layer and the electrons are pushed along the force direction and locally separated from the plasma ions. The system of the electron layer and the ion layer creates the so-called double layer (e.g., [67,68]), which is a region of non-neutral plasma where a large potential drop generates a very strong electric field (the charge separation field) that accelerates the ions. Since, in general, two oppositely directed ponderomotive forces are induced in the skin layer, these forces drive (via the double layer mechanism) two ion bunches moving in the forward and backward directions. This ion acceleration mechanism is sometimes called skin-layer ponderomotive acceleration (SLPA) [7,46–48]. This mechanism can effectively accelerate ions at both relativistic and sub-relativistic laser intensities. In the case where the laser pulse intensity is sufficiently high ($>10^{20}$ W/cm^2) and the pre-plasma density gradient is high, the forward ponderomotive force (ponderomotive or radiation pressure) clearly prevails over the backward one and only a high-density forward-accelerated (along the laser beam axis) ion bunch is actually produced and accelerated. This high-intensity case of the SLPA mechanism is usually called radiation pressure acceleration (RPA) [1–4,36–45].

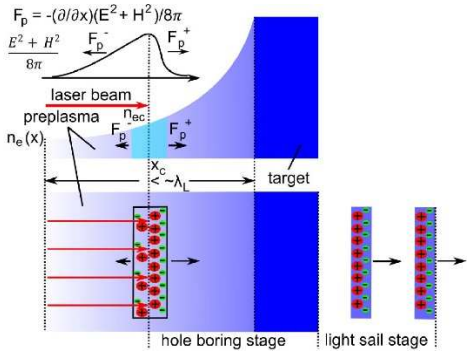

Figure 1. The idea of ion acceleration by the RPA mechanism. F_p—ponderomotive force; E, H—strength of the electric and magnetic field, respectively of the laser beam in the plasma; n_e—electron density in the plasma; n_{ec}—critical electron density; x_c—position of the critical density surface.

In the RPA mechanism, two stages/regimes of ion acceleration can be distinguished, namely, the hole-boring (HB) stage and the light-sail (LS) stage (Figure 1) [1,2]. In the HB stage, ions from the front part of the target are accelerated towards the interior of the target by the charge separation field of the forward-moving double layer driven by the pressure of laser radiation. The increase in ion energy is accompanied by an increase in the number of accelerated ions, because the moving (positively charged) ion layer in the double layer acts as a piston on the ions stored in the undisturbed part of the target. The HB stage ends when the ion (plasma) bunch generated in this way reaches the rear surface

of the target. After the ion bunch crosses this surface, the LS stage begins. In this stage, the ion bunch is accelerated by the radiation pressure in free space similar to a sail pushed by the wind. Depending on the target thickness and the laser fluence F_L, RPA-HB or RPA-LS dominates the ion acceleration process. When the target is thick enough (or the F_L is not high enough), almost all of the laser energy is used to accelerate ions inside the target, and thus the acceleration process is dominated by RPA-HB. Optimal conditions for RPA-HB occur when the target thickness $L_T \approx L_{HB} = \tau_L V_{HB}$, where V_{HB} is the average recession velocity of the plasma (ion) surface driven by the laser piston and τ_L is the laser pulse duration. Since $V_{HB} \sim A^{-1/2}$ [2], the optimal target thickness for this acceleration regime decreases proportionally to $A^{-1/2}$, and for super-heavy ions, it is by a factor of ~4 smaller than for light ions such as carbon ions. Approximate analytical formulas for estimating the energy of ions accelerated by RPA-HB can be found, e.g., in [2]. In contrast, when the target is thin enough (or the F_L is high enough), only a small part of the laser energy is used to accelerate ions inside the target and the majority of the laser energy are used to accelerate the ion bunch in free space behind the initial target position. Thus, the acceleration process is dominated by RPA-LS. As shown in [69], in order for ion acceleration to be realised in the RPA-LS regime, the following condition should be met: $1/4\ L_{skin} < L_T < 5\ L_{skin}$, where $L_{skin} = \gamma^{1/2}\ c/\omega_p$ is the relativistic skin depth of the plasma ($\gamma \sim {I_L}^{1/2}$—relativistic parameter; ω_p—electron plasma frequency; c—speed of light). When $L_T < 1/4\ L_{skin}$, the acceleration is inherently unstable and corresponds to the CEA regime, while when $L_T > 5\ L_{skin}$, the TNSA-like mechanism dominates. The most efficient acceleration takes place when $L_T \sim (1–2)\ L_{skin}$, provided that the laser pulse is not very long and the transverse expansion of the plasma during the pulse is small. A convenient analytical formula for estimating the energy of ions accelerated by RPA-LS when the laser pulse energy fluence, F_L, and the target areal density, σ, are known can be found in [2].

The most important advantages of the RPA mechanism are as follows [1–4]: (1) RPA enables the efficient acceleration of both light and heavy ions and laser-to-ions energy conversion efficiency can be very high (can reach several dozen percent). (2) Scaling of the RPA-driven ion energy with the laser intensity/fluence is very favourable ($E_i \sim (I\tau)^{\alpha}$, where $\alpha = 2$ for $v_i << c$, and $\alpha = 1$ for the LS mode or $\alpha = 1/3$ for the HB mode at $v_i \approx c$); this potentially enables reaching relativistic ion energies of the order of tens of GeV for light ions and up to TeV for heavy ions. (3) The areal ion density, σ_i, at the source can be high (up to $\sigma_i \geq 10^{20}$ cm^{-2}) which enables achieving very high ion beam intensities and fluences also at moderate ion energies. (4) It is possible to produce ultra-short ion pulses with durations from tens of fs to ps. (5) The ion beam can have a quasi-monoenergetic ion energy spectrum.

RPA also has a number of disadvantages, particularly the following: (1) Achieving high acceleration efficiency usually requires very high laser intensities (>10^{21} W/cm^2) and a high laser pulse contrast ratio. (2) The transverse homogeneity of the laser beam driving the ions should be high. (3) Circularly polarised laser beams usually provide higher acceleration efficiency and better quality of the generated ion beam than the more easily produced linearly polarised laser beams. (4) Rayleigh-Taylor-like (and other) instabilities can occur in the acceleration process and negatively affect the acceleration efficiency and quality of the generated ion beam.

It should be added that due to the high requirements for the laser beam driving ions in the RPA regime, and mainly the requirement of very high laser intensity, experimental studies of RPA are still at an early stage. Current knowledge about the properties of the RPA mechanism and ion beams driven by this mechanism is mainly the result of theoretical and numerical studies. It can be believed that the rapid development of ultrafast multi-PW

lasers observed in recent years will significantly accelerate experimental research on ion acceleration by RPA as well as on possible applications of the generated ion beams.

2.2. Ion Acceleration by the Target Normal Shield Acceleration (TNSA) Mechanism

The second acceleration mechanism that has a significant impact on the acceleration process and the properties of the heavy ion beam is the TNSA mechanism [1–4,26–35]. The idea of this mechanism is illustrated in Figure 2. A short, pico- or femtosecond laser pulse irradiating the front surface of the target produces plasma and a stream of hot (fast) electrons with a temperature T_h usually in the range of ~0.1–10 MeV. The electrons penetrate the target and form a Debye sheath on its rear surface, which acts as a virtual, moving cathode. The electric field induced by the cathode: $E_{ac} \sim T_h/e\lambda_{Dh} \sim 1$–$100$ GeV/cm (λ_{Dh} is the Debye length) is very high and easily ionises atoms accumulated in a thin (~5–10 nm) layer on the rear surface of the target. The ions generated in this way are accelerated by the virtual cathode at a distance of $L_{ac} \sim 10$–100 μm to an energy of $E_i \sim ZeL_{ac}E_{ac} \sim 1$–$100$ MeV (Z is the charge state of the ion). The ions are accelerated mainly in directions close to the normal to the back surface of the target and, as a result, the angular divergence of the ion beam is relatively small.

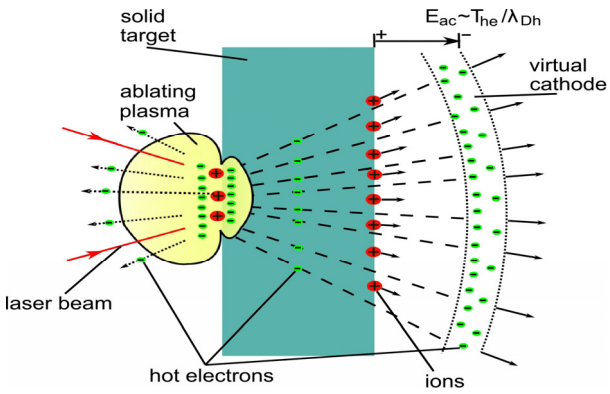

Figure 2. The idea of ion acceleration by the TNSA mechanism (see the text).

The TNSA mechanism can effectively accelerate ions with a high Z/A ratio. It is therefore effective primarily in accelerating protons (Z/A = 1) and highly ionised light ions (e.g., Be, Li, C) for which $Z/A \approx 1/2$ [1,2]. Protons and such light ions can be generated both from insulators (e.g., polyethylene, polystyrene) and metal targets, the thickness of which is usually in the range of 0.1–10 μm. When a metal target is used, the source of protons and light ions is usually hydrocarbon impurities (H, C), which are almost always present on the target surfaces and are efficiently ionised by the TNSA field (sometimes, the back surface of the target is covered with a thin layer of CH or CH_2 [70]). In the case that the goal is to accelerate protons or light ions from metal targets, the low-Z impurities present in these targets are desirable and even essential. However, when the goal is to accelerate heavy ions from high-Z metal targets, these impurities play a negative role, as a significant part of the laser energy is spent on accelerating light ions or protons, which in turn can significantly reduce the efficiency of heavy ion acceleration.

Regardless of the composition and structure of the target, usually only ions from a very thin ($\leq$10 nm) layer on the rear surface of the target are efficiently accelerated by the TNSA mechanism. As a result, the areal density σ_i of the ion source is relatively small, $\sigma_i < 10^{17}$ cm^{-2}, and the ion density in the source n_i is moderate, $n_i < 10^{19}$ cm^{-3}. Thus, achieving high ion beam intensities $I_i = n_i v_i E_i$ (say $>10^{18}$ W/cm^2) and/or energy fluences $F_i = \sigma_i E_i$ (say $F_i > 1$ MJ/cm^2) is possible only at very high ion energies ($E_i \sim 100$ MeV or higher). On the other hand, the total number of accelerated ions can be fairly high (up to

N_i ~ 10^{12}–10^{13} [1,2,71]), because due to the transverse transport of fast electrons in the target, the size of the surface from which ions are extracted and accelerated is much larger than the size of the laser beam on the target.

Ion acceleration using the TNSA mechanism has a number of advantages, particularly the following: (1) Moderate requirements for the laser beam quality (both the beam transverse distribution and the laser pulse contrast) and intensity (both relativistic and sub-relativistic laser intensities can be used), as a result, proton beams with energies of ~100 MeV can be generated at currently achievable laser intensities. (2) Very low transverse emittance of the ion/proton beam. (3) Good quality of the transverse energy distribution in the ion/proton beams.

The TNSA method, however, also has a number of disadvantages, which include the following: (1) A wide (quasi-Maxwellian) ion energy spectrum. (2) Relatively low efficiency of laser energy conversion into ion/proton energy (typically ~1%, although under certain conditions it is possible to achieve an efficiency of 15% [72]). (3) A relatively slow increase in the maximum ion energy E_{imax} with the increasing laser intensity: $E_{imax} \sim (I_L)^{0.5}$ [1,2]. (4) A relatively low areal density of ions in the source ($<10^{17}$ cm^{-2}), which makes it difficult to achieve very high intensities and fluences of the ion/proton beam at achievable laser intensities. Despite these disadvantages, TNSA is still the most effective and recognised method of proton acceleration with the potential to produce high-quality proton beams.

The above-mentioned advantages of TNSA, and in particular, the not very high requirements for laser intensity and beam quality, as well as the possibility of using simple targets that do not require sophisticated technologies, make TNSA the best-known mechanism so far, and ion beams produced by this method have a significant application potential. This, in turn, stimulates further development of research on this acceleration method, in particular, in terms of increasing the acceleration efficiency, increasing the ion energy, and improving the quality of the ion beam.

The significance of TNSA in the heavy ion acceleration process depends to a large extent on the laser intensity. At relativistic but moderate intensities of ~10^{21} W/cm^2 and lower, TNSA can be the dominant mechanism in this process. At such laser intensities, low-Z impurities present on the surface of the high-Z target play an important role, which, as explained above, are effectively accelerated by TNSA and can cause a significant decrease in the efficiency of heavy ion acceleration [73,74]. To increase this efficiency, target cleaning from impurities is often used in this case. With the increasing laser intensity, the role of RPA mechanism in heavy ion acceleration increases (especially when the laser beam is circularly polarised) and, at ultra-high laser intensities of ~10^{23} W/cm^2 and higher, this acceleration mechanism dominates and determines the most important parameters of the ion beam such as mean ion energy, beam fluence and intensity [5,64–66]. However, also in this case, TNSA plays a significant role, especially in the post-RPA stage of acceleration where TNSA is the dominant mechanism [5,64,65]. At ultra-high laser intensities, the influence of low-Z impurities on the heavy ion acceleration process is usually small mainly due to the small energy carried by light ions compared to the total energy of heavy ions acquired in the RPA stage of acceleration [64–66].

2.3. Ion Acceleration by the Coulomb Explosion Acceleration (CEA) Mechanism

When a laser pulse of sufficiently high intensity of the order of 10^{21}–10^{22} W/cm^2 or higher interacts with thin targets [1], a gas containing sub-micrometre solid clusters [1,51,52] or, for example, a subcritical plasma from the region of a self-focusing plasma channel [53], it becomes possible to accelerate ions by the Coulomb explosion mechanism. In such a case, the electromagnetic field of the laser pulse acting directly on the electrons contained in the plasma is able to knock out a significant number or even all of the electrons from a

given area (target, cluster or channel), leading to the breaking of the electrical neutrality of the plasma. This leads to the formation of an area with a positive electrical charge and a gradual increase in the electrical potential in the region along with the removal of electrons from it. The maximum value of such potential can be estimated (on the example of a cluster) at: $\varphi_{max} = \frac{R^2 nq}{3\varepsilon}$, where n is the density of ions, q is the ion charge, R is the radius of area, and ε is permittivity [51]. This leads to the creation of an electric field associated with this electric potential that accelerates ions from the discussed region in all directions. In Figure 3, we can see an example of such field associated with the Coulomb explosion acceleration mechanism. We can clearly see part of the field accelerating ions forwards and backwards. Additionally, it can be seen that in the case of ions with a high level of ionisation, even a small relative loss of electrons can lead to a Coulomb explosion.

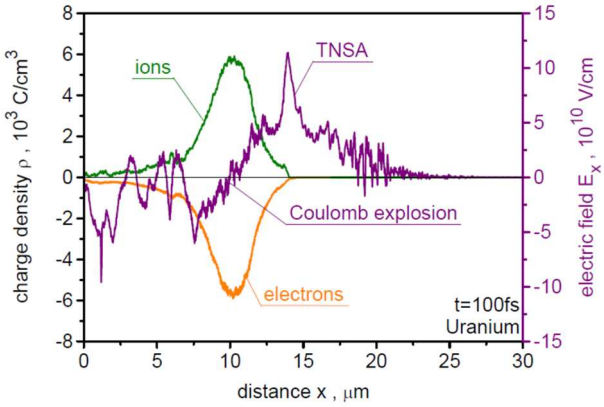

Figure 3. Cross-section along the x axis for the two-dimensional electron and ion charge distributions, as well as the x component of the electric field-accelerated ions in the plasma. Results of the 2D PIC simulation of acceleration of uranium ions from a 51-nm thick uranium target irradiated by a 30-fs laser pulse with an intensity of 10^{23} W/cm^2. t = 100 fs is the simulation time.

The time needed to remove electrons from the considered region depends on the intensity of laser pulses. In a situation where φ_{max} is negligible with respect to the kinetic energy of electrons, they can be removed from the considered region in time $\delta t \approx R/c$. For this to happen, the following condition must be met: $a > \sqrt{2/3}(R/d_e)(\omega_{pe}/\omega)$ where a is the dimensionless amplitude of laser field, $d_e = c/\omega_{pe}$ is the collisionless skin depth, ω_{pe} is the plasma frequency, and ω is the laser frequency (considerations on the example of a spherical cluster). This means that for $R = 1$ μm and $n = 10^{23}$ cm^{-3}, the laser pulse intensity of 10^{24} W/cm^2 is needed. For lower laser pulse intensities, the electron ejection process takes place during time $t = 2\pi(R/r_E)\omega^{-1}$, where $r_E = d_e a(\omega/\omega_{pe})$ is the quiver radius of electron inside the cluster [51]. In order for ion acceleration by the CEA mechanism to occur effectively, the target/cluster cannot be too thick/large because the laser pulse will have difficulty knocking out a sufficiently large number of electrons. They also cannot be too thin/small because then, even if all the electrons are knocked out, the charge of the remaining ions will be too small to generate a sufficiently strong field. The optimal situation corresponds to the case in which the maximum value of the field associated with the CEA mechanism, located at the edge of the electron loss region, is close to the maximum value of the electric field of the laser pulse. This means that there is an optimal size for the target: $\sigma_{opt} = 0.4a + 3$, where $\sigma = \frac{n_e l}{n_{cr}\lambda}$, n_e is the electron density of the target, n_{cr} is the plasma critical density, l is the target thickness, and λ is the laser wavelength. The optimal cluster size is as follows: $R = 3an_{cr}\lambda/(2\pi n_e)$ [1]. It is clear that for both cases, the optimal value (from the point of view of the CEA mechanism) is linearly dependent on the laser pulse intensity and inversely proportional to the electron density. Simple substitutions also show that considering a cluster/target with a density close to that of a solid state and a

laser pulse with an intensity of the order of 10^{22} W/cm^2 in both cases, we need dimensions much smaller than the laser pulse wavelength [1].

To sum up, in the real process of laser-driven acceleration of ions, including heavy ions, several acceleration mechanisms usually contribute. Which of these mechanisms has a significant or dominant contribution to this process depends on the laser and target parameters, including intensity, polarisation, wavelength, contrast ratio, duration and quality of the laser beam and the thickness, density, structure, quality, etc. of the target. This contribution also depends on the pre-plasma parameters, including thickness, shape of the spatial density distribution (in particular, the density gradient) or the type (atomic composition) of the pre-plasma. This applies, in particular, to the contribution of the RPA and TNSA mechanisms to the acceleration process, i.e., mechanisms that play the most important role in the acceleration of heavy ions to high energies (multi-GeV and higher). Due to the large number of parameters that determine the contribution of a given mechanism to this process, it is difficult to clearly determine under what conditions the contribution of this mechanism is significant/dominant or under what conditions a transition from one mechanism to another occurs (a rough determination of such conditions is sometimes feasible, but with a significant narrowing of the number of laser–target interaction parameters, e.g., [69,75]). However, it is possible to indicate what conditions favour a significant/dominant contribution of a given mechanism to the acceleration process, including the RPA and TNSA mechanisms. In particular, efficient ion acceleration by RPA is supported by high laser intensity (>>10^{21} W/cm^2) [1,2], circular polarisation of the laser beam [1,2], short laser wavelength [1,2,76], high contrast ratio [2,40,44], high quality of the laser beam (especially its spatial distribution) [77,78], rather small target thickness (in the range of sub-um thicknesses matched to the laser intensity) [2,69], and high pre-plasma density gradient [2,40]. Efficient ion acceleration by the TNSA (or TNSA-like) mechanism is possible with much lower requirements for the laser and target than for RPA. This mechanism can be particularly efficient at both relatively low (~10^{19}–10^{20} W/cm^2) and high (including ultra-high) laser intensities [1,2,64,65] and using both micrometre and sub-micrometre targets [1,2]. Furthermore, the quality of the laser beam (its spatial distribution) does not necessarily have to be very high (although, of course, the high quality of this beam favours obtaining a high quality ion beam). The efficiency of TNSA is favoured by a linear polarisation of the laser beam, a long laser wavelength and a moderate pre-plasma density gradient [1,2]. RPA and TNSA often compete with each other in the acceleration process and depending on the laser and target parameters, either RPA or TNSA dominates in this process. Sometimes, however, each of these mechanisms plays a dominant role in this process, but at different stages of acceleration: RPA dominates in the stage of direct interaction of the laser with the target/plasma, while TNSA dominates in the post-RPA stage, i.e., after the end of this interaction (e.g., [64,65]). The general properties of the ion acceleration process outlined above occur in the case of both light and heavy ion acceleration.

In the next two sections, we review the major results of studies on heavy ion acceleration driven by ultrafast high-peak-power lasers performed over a wide range of laser intensities from ~10^{16} W/cm^2 to ~10^{24} W/cm^2. For the purposes of this paper, we have divided this range into two sub-ranges: moderate and high intensities, i.e., from >10^{16} W/cm^2 to <10^{23} W/cm^2 (Section 3) and ultra-high intensities, i.e., $\geq 10^{23}$ W/cm^2 (Section 4). The reasons for dividing laser intensities into these two sub-ranges are primarily technical/practical but partly also physical. The first divides intensities into those currently achievable (moderate and high intensities) and those that will be achievable in the future (ultra-high intensities). For this reason, in Section 3 mainly (but not exclusively) experimental studies are discussed, while in Section 4 (ultra-high intensities) only theoretical

and numerical results are presented. The division adopted roughly coincides with the division into two ranges of laser intensities in which particles accelerated in the plasma are relativistic or non-relativistic particles. In the range of intensities called here moderate and high intensities, only electrons accelerated by the fields induced by the laser in the plasma can reach relativistic velocities, while ions are non-relativistic particles. In the ultra-high intensity range, both electrons and ions can be accelerated by these fields to relativistic velocities. Of course, the boundary between these ranges is not sharp and in this sense the division into these two ranges is rather conventional, but useful for the purposes of our article.

3. Acceleration of Heavy Ions at Moderate and High Laser Intensities

As explained in Section 2, at laser intensities exceeding 10^{16} W/cm^2, the motion of ions in a laser accelerator is primarily determined by quasi-static electric fields induced by the laser in the accelerator plasma. The efficiency of ion acceleration in an electric field depends on the ratio of the ion charge to its mass, i.e., on the Z/A ratio and increases with the increase in this ratio. Therefore, in order to achieve high acceleration efficiency, one should strive to achieve high values of the Z/A of the ion, which is particularly important in the case of heavy ions. Since the atomic number for heavy elements Z_a is always less than half the total number of protons and neutrons in the atomic nucleus, only with very high charge states Z close to Z_a can we achieve high acceleration efficiency close to that for light ions, usually for which $Z/A \approx 1/2$ (for protons $Z/A = 1$). The key issue in the acceleration of heavy ions, and especially super-heavy ions, is therefore the production in the laser–target interaction process of ions with the highest possible charge state Z. In the case of long laser pulses (sub-ns, ns or longer), achieving high Z values is possible even at relatively low laser intensities (~10^{13}–10^{16} W/cm^2). In this case, the basic ionisation mechanism is electron–ion collisions in the plasma. The long lifetime of the plasma generated by a long-pulse laser (comparable to the laser pulse duration) and relatively high density (>10^{20} cm^{-3}) and temperature (up to several keV) enable achieving charge states of heavy ions in this plasma reaching Z ~ 50–70 [7,79,80]. However, the ion energies at these laser intensities are rather low, usually in the range of 1–100 MeV. On the other hand, long-pulse high-energy (~100–1000 J) lasers make it possible to generate ion streams containing a large number of highly charged ions (up to 10^{14}–10^{15}) and with high peak ion currents (up to ~100 A) and ion current densities (up to several A/cm^2 at 1 m from the ion source) [81].

Research on heavy ion acceleration driven by ultrafast lasers, i.e., lasers generating pico- or femtosecond pulses, began at the turn of the twentieth and twenty-first centuries, when ultrafast lasers with TW and multi-TW powers became widely available. In the first period of this research, the focus was on the acceleration of heavy ions in the direction opposite to the direction of laser beam propagation (backward direction) produced from relatively thick targets (several dozen μm or thicker). This was due, on the one hand, to the limited access of most researchers to advanced target fabrication technologies (including fabrication of sub-micrometre or nanometre thick targets), and on the other hand, to the rather moderate laser intensities available at that time, covering the range of sub-relativistic and low-relativistic intensities (~10^{18}–10^{19} W/cm^2). With the increase in power (up to PW and multi-PW) and intensities (up to 10^{21}–10^{22} W/cm^2) of laser beams and the easier access to ultra-thin targets and targets with complex structures (see e.g., [82]), the interest of researchers shifted towards the study of forward-accelerated heavy ion beams. Forward accelerated ion beams may have significantly more advantageous properties than backward-generated beams and are more useful in a variety of potential applications. In Sections 3.1 and 3.2, the results of experimental studies on the backward (Section 3.1) and forward (Section 3.2) acceleration of heavy ions by ultrafast lasers in the range of laser

intensities from sub-relativistic to relativistic up to 10^{22} W/cm^2 are briefly summarised. This summary includes only some selected results of heavy ion acceleration studies to date, considered by the authors to be representative of this field of research, and does not pretend to be an exhaustive review.

3.1. Backward Acceleration of Heavy Ions

The results of some of the first experiments investigating the backward acceleration of heavy ions driven by a picosecond laser pulse of sub-relativistic intensity were presented in [83–86]. In these studies, an ultrafast neodymium terawatt laser generating a pulse of 1 ps duration, energy of 0.5–1 J, and laser beam intensity on the target in the range of 10^{14}–10^{17} W/cm^2 was used. Using a diagnostic system containing an electrostatic ion energy analyser (IEA) and a set of ion collectors, the energy and charge state of ions generated backward from massive (thick) metal targets of different atomic numbers were studied. In [83], ion fluxes from a copper target were studied. Cu ions with charge states Z from 1 to 13 were detected by IEA. The ions were generated in two groups: the fast ion group and the low-energy (thermal) ion group. It was found that in the studied range of sub-relativistic laser intensities I_L, the mean energy, E_{mean}, of fast ions increases linearly with the increasing I_L and reaches a maximum value of ~300 keV, while E_{mean} for thermal ions increases with intensity proportionally to $(I_L)^{1/2}$ and reaches values below 50 keV. In [84], Ag ion fluxes generated backward at a laser intensity of 5×10^{16} W/cm^2 were studied. Highly charged Ag ions with a maximum charge state of $Z_{max} = 29$ and $E_{max} = 0.9$ MeV were measured. Backward emission of ions from targets with various atomic numbers in the range from 13 (Al) to 79 (Au) was studied in [85]. The most important results of this work are summarised in Table 1, which presents the measured values of Z_{max}, E_{max}, and peak ion current densities measured at one metre from the target, j_{max}, for Al, Fe, Cu, Ag, Ta and Au ions.

Table 1. Maximum charge states, Z_{max}, maximum energies, E_{max}, and peak ion current densities measured at 1 m from the target, j_{max}, for heavy ion beams accelerated backward by a 1-ps laser pulse with an intensity of $I_L = 5 \times 10^{16}$ W/cm^2 and energy of $E_L = 0.45$ J.

Element	Al	Fe	Cu	Ag	Ta	Au
Z_{max}	13	18	17	29	38	33
E_{max}, MeV	0.1	>0.2	≥0.3	0.9	~1	~1
j_{max}, mA/cm^2	3.3	-	2.2	3.2	1.3	0.8

The highest charge states were measured for the heaviest ions: Ta ($Z_{max} = 38$) and Au ($Z_{max} = 33$). Au and Ta ions also reached the highest energies approaching 1 MeV. Current densities of the studied ions at a large distance from the ion source (1 m) were quite high ~>1 mA/cm^2, and the angular divergence of the ion flux did not exceed 30 degrees.

In [86], the properties of Au ion streams generated by 1 ps and 0.5 ns pulses with similar energies and focal spots on the target were compared. It was found that although the laser intensities for 1 ps and 0.5 ns pulses differ significantly (8×10^{16} W/cm for 1 ps vs. 2×10^{14} W/cm^2 for 0.5 ns), the maximum charge states and mean energies of Au ions are comparable for these pulses ($Z_{max} = 26$ vs. $Z_{max} = 32$ and 17 keV/u vs. 19 keV/u). However, other properties of ion streams generated by ps and sub-ns pulses, as well as ion acceleration mechanisms, differ significantly. In the case of the ps pulse, only one fast ion group with small angular divergence (~10 degrees, FWHM) is generated and the probable acceleration mechanism is the SLPA mechanism. In the case of the sub-ns pulse, two or more fast ion groups are generated in a wide solid angle (~60 degrees) and it seems that the ion flux properties are largely determined by the self-focusing of the laser beam in the plasma.

Although in works [83–86] the mechanisms of target plasma ionisation and the formation of highly charged ions were not studied, based on the current knowledge, it can be assumed that the dominant ionisation mechanism was electron–ion collisions. As for the ion acceleration process, not only the SLPA mechanism but also the TNSA-like mechanism arising from the escape of hot (fast) electrons from the plasma could contribute to this process.

It is worth adding that these works also demonstrate the ability to produce highly charged ion fluxes with MeV ion energies by ultrafast low-energy lasers (~1 J), which are currently capable of operating with a high repetition rate (>1 Hz). This opens up the possibility of using such ion fluxes in some applications, such as ion implantation in near-surface layers of materials to improve their properties.

The first, to our knowledge, experiment demonstrating backward acceleration of heavy ions at relativistic laser intensity was presented in [87]. In this experiment, a 1-ps Nd laser pulse with an intensity of 5×10^{19} W/cm^2 was used to illuminate a thick (2 mm) lead target. Using a Thomson parabola spectrometre (TPS), highly charged Pb ions with Z_{max} = 46 and peak energy E_{max} = 430 MeV were detected. It was suggested that the acceleration of Pb ions is a combination of a Coulomb explosion (CEA mechanism) and acceleration by the space charge force from hot electrons which escape the plasma (TNSA-like mechanism).

In [88], the acceleration of ions from a 100-μm iron target driven by a 0.7-ps laser pulse with an intensity of 2×10^{20} W/cm^2 was investigated. The activation method using the ^{56}Fe + ^{12}C fusion–evaporation reactions was used to estimate the energy of Fe ions. From the activation measurements, the maximum energy of Fe ions was deduced to be about 330 MeV for the unheated iron target and ~650 MeV for the target heated to a temperature of 860 Celsius degrees. According to the authors, this almost two-fold increase in the energy of Fe ions from the heated target was the result of the removal of hydrocarbon contaminants from the target surface, which significantly reduced the efficiency of heavy ion acceleration.

More detailed studies of heavy ion acceleration were carried out in [89]. The backward and forward acceleration of Pd ions generated from a 25-μm thick palladium target illuminated by a laser pulse from 1 to 8 ps duration and intensity in the range of 5×10^{19}–5×10^{20} W/cm^2 was studied. It was found that the backward ion stream contains more ions and higher charge states than the forward stream, while the maximum ion energies are similar in both directions. For a laser intensity of 2×10^{20} W/cm^2, Pd ions with Z_{max} = 30 and $E_{max} \approx 400$ MeV were detected in the backward stream. The dependence of the maximum Pd ion energy on the laser intensity I_L was studied and it was shown that E_{max} increases proportionally to $(I_L)^{1/2}$.

For backward acceleration of heavy ions at relativistic laser intensities, lasers generating femtosecond pulses have also been used. An example is the work [90], in which a femtosecond laser pulse (25–45 fs) with an intensity of 10^{18}–2×10^{19} W/cm^2 illuminates an Au-C-Al (or Si) nano-composite target containing Au nanoparticles. It has been shown that in such a laser-target set, it is possible to generate Au ion streams with a narrow energy spectrum (energy spread < 10%), the number of ions up to 9×10^{10} per shot, and the maximum ion energy of ~0.5 MeV. According to the authors, the heavy ion stream with the above properties is produced by the thermal pressure of the expanding hot plasma, and not by the electric field induced by hot electrons escaping from the plasma. The results quite similar to those presented in [90], in particular, the generation of Au ions with a narrow energy spectrum and a maximum energy of ~0.5 MeV were obtained in [91], where a multi-layer target containing nanometre-sized Au (5 nm) and C (10–40 nm) layers deposited on a 1-mm thick Si substrate was used. The relatively low energy of the ions achieved in these works can be explained by the rather low fluence of the laser pulses used,

comparable to the fluence of the picosecond pulse of sub-relativistic intensity used in the experiments [83–86].

Table 2 summarises the quantitative results of the experiments discussed in this sub-section, relating to the achieved maximum energies and charge states of the accelerated ions. These experiments were carried out in very different physical conditions, in which the differences concerned not only the intensity and duration of the laser pulse and the base target material, but also other parameters influencing the laser–target interaction process, such as the laser pulse intensity contrast or the target structure and thickness. Therefore, the results presented in the table cannot be the basis for determining, for example, the rules for scaling E_{max} or Z_{max} changes with increasing laser intensity. Despite this, we have grounds to state that the simultaneous increase in laser intensity and fluence results in a fairly fast (but slower than linear) increase in the maximum energy of heavy ions accelerated backwards, which at a picosecond pulse intensity of ~10^{20} W/cm^2 results in the acceleration of heavy ions to sub-GeV energies. On the other hand, in the considered range of laser intensities, the influence of intensity/fluence on the achieved maximum charge state of the ion is small and the value of Z_{max} is primarily determined by the atomic number and the energy level structure of the ionised atom.

Table 2. Maximum charge states, Z_{max}, and maximum energies, E_{max}, of heavy ions accelerated backward by an ultrafast laser. I_L, τ_L, and E_L are the intensity, duration, and energy of the laser pulse, respectively.

Element	Z_{max}	E_{max}, MeV	I_L, 10^{18} W/cm^2	τ_L, ps	E_L, J	References
$^{207}Pb^{82}$	46	430	50	1	50	[87]
$^{197}Au^{79}$	33	~1	0.05	1	0.45	[85]
$^{197}Au^{79}$	26	>1	0.08	1	0.45	[86]
$^{197}Au^{79}$	~10	~0.45	20	0.025	~1	[90,91]
$^{181}Ta^{73}$	38	~1	0.08	1	0.45	[85]
$^{108}Ag^{47}$	29	0.9	0.05	1	0.5	[84]
$^{106}Pd^{46}$	30	400	200	1	120	[89]
$^{64}Cu^{29}$	13	≥0.3	0.63	1	0.5	[83]
$^{56}Fe^{26}$	18	>0.2	0.05	1	0.45	[85]
$^{56}Fe^{26}$		650	200	0.7	400	[88]

3.2. Forward Acceleration of Heavy Ions

Progress in ultrafast laser technology resulting in increased power and intensity of pico- and femtosecond pulses as well as mastering the technology of producing ultra-thin targets (~10–100 nm thick) has caused a shift in the interest of researchers involved in laser acceleration of heavy ions from backward acceleration to forward acceleration of ions. Forward acceleration can potentially ensure the production of heavy ion beams with ion energies and other parameters higher than for backward accelerated beams and to a greater extent meet the requirements of various applications of these beams. Research on forward acceleration of heavy ions, both experimental, theoretical, and numerical, has developed primarily in the last ten years. During this period, a number of experiments and numerical studies of heavy ion acceleration for high laser intensities in the range of 10^{20}–10^{22} W/cm^2 were performed. In this sub-section, we will briefly summarise the most significant results of these studies, including the achieved energies and measured charge states of heavy ions.

The paper [92] reports the results of Fe ion acceleration by a 35-fs laser pulse with an energy of 8 J and intensity of 10^{21} W/cm^2. The ion source was iron impurities on the surface of a 0.8-um thick Al target. Highly charged Fe ions with a maximum energy of 0.9 GeV accelerated by the TNSA mechanism were demonstrated.

In [93], the acceleration of Au ions from an ultra-thin (14 nm) gold foil was studied. The foil was irradiated by a 35-fs laser pulse with an energy of 1.6 J and an intensity of 8×10^{19} W/cm^2. Au ions with a maximum energy of $E_{max} \approx 200$ Mev and a maximum charge state of $Z_{max} \approx 50$ were recorded. Based on theoretical models and particle-in-cell (PIC) simulations, it was found that the dominant mechanism of ionisation of gold atoms is ionisation by the laser field, while the acceleration of highly charged Au ions is significantly enhanced by the Coulomb explosion of ions.

The results of the experiment with Au ion acceleration driven by a sub-picosecond (0.14 ps) laser pulse with an intensity of 8×10^{20} W/cm^2 and energy of several dozen J are presented in [94]. In the experiment, the energy spectra of Au ions from a gold target of 50, 100, and 300 nm thickness were compared for the case of a cold target and a target heated to 500 degrees in order to remove low-Z impurities from the target surface. Based on measurements using the Thomson parabola spectrometre (TPS), it was found that in both cases, the energy spectrum has a shape suggesting the dominance of the TNSA mechanism in ion acceleration, with the maximum energies of ions generated from heated targets being higher by a factor of 1.2–1.5 than those of ions produced from cold targets and reaching 1 GeV. However, no significant effect of target heating on the maximum value of the ion charge state was found, and for the target thickness of 100 nm, ions with $Z_{max} \sim 50$ were detected in both cases.

In [95], the acceleration of Ag ions from silver targets with thickness in the range of 50–800 nm was studied. The ions were driven by a femtosecond (40 fs) laser pulse with an intensity of 5×10^{21} W/cm^2 and energy of ~10 J. The acceleration of highly charged ($Z_{max} = 45$) Ag ions to energy of ~2.2 GeV was demonstrated. The measurements were supported by detailed 2D PIC simulations which allowed for a deeper insight into the ionisation and acceleration mechanisms of ions. It was found that although for lower charge states ($Z < 38$) the ions can be either field or collisional ionised, for targets thicker than 500 nm, the dominating ionisation mechanism for high charge state ($Z = 38$–47) Ag ions is collisional ionisation. Meanwhile, for the thinnest target (50 nm) field ionisation dominates, albeit with a significant contribution from collisional ionisation. The dominant mechanism of Ag ion acceleration is TNSA; however, for the thinnest target, the influence of the RPA-HB mechanism is noticeable. The latter results in higher energy and charge state of ions but leads to target deformation and makes it difficult to control the parameters of the generated ion beam. It has also been shown that the laser pulse rising edge with relativistic intensity and length of several hundred fs can effectively remove light contaminants from the surface of a thin target, and thus increase the efficiency of heavy ion acceleration.

The paper [12] reports the acceleration of Au ions by a femtosecond (22 fs) laser pulse with an intensity of 1.1×10^{22} W/cm^2, the highest used in heavy ion acceleration experiments performed to date. Using a double-layer target composed of a 60-µm carbon nanotube foam (CNF) layer and a 150-nm gold layer, the acceleration of Au ions with $E_{max} = 1.2$ GeV and $Z_{max} = 61$ was demonstrated. The ion energies from the double-layer target were a factor of ~1.7 higher than those achieved with the single-layer Au target. Based on 2D PIC simulations, it was found that the main reason for the increased ion energy from the double-layer target is the extension of the ion acceleration time due to the presence of the CNF layer.

A similar experiment as in [12] but with a much longer pulse of 0.5 ps duration was performed in [96], where a laser pulse with an intensity of 4×10^{20} W/cm^2 and energy of about 180 J irradiated an Au target (heated or unheated) of thickness 25, 45, 100, 300 or 500 nm. The measured energy spectra and charge state distributions of Au ions showed a significant dependence on the target thickness. The highest ion energies with $E_{max} = 1.4$–1.5 GeV and the highest Au ion charge state $Z_{max} = 72$ were measured for the heated target of thickness

100 nm. It was noted that the achieved value of Z_{max} is the highest among the Au ion charge states measured so far in experiments with laser-driven acceleration of heavy ions, the value of Z_{max} = 72 for Au was also measured in [97], but in a different type of experiment.

It was found that the recorded charge state distributions of Au ions are difficult to explain using the established ionisation models applied in studies on laser acceleration of heavy ions.

The results of the study of the acceleration of Au ions driven by a high-energy sub-picosecond laser were also reported in [98,99]. In [98], a laser pulse of 0.85 ps duration, intensity of (3–5) $\times$ 10^{20} W/cm^2, and energy of 200 J irradiated a gold target of several dozen nm thickness. Au ions with a maximum energy of 1.6 GeV and a charge state of +58 were detected.

In [99], the Au ion fluxes generated from an ultra-thin (15 nm or 30 nm) gold target irradiated by a 0.8-ps laser pulse with an intensity of ~3 $\times$ 10^{20} W/cm^2 and energy of ~175 J were measured. In the case of the 15 nm target, the energy spectra of Au ions with a distinct quasi-monoenergetic peak extending from 1 GeV to 2 GeV with mean energy ~ 1.5 GeV and the number of ions on the order of 10^{12} particles per steradian were recorded. According to the authors, this was the first experimental observation demonstrating laser-driven generation of a quasi-monoenergetic beam of super-heavy ions. Particle-in-cell numerical simulations have shown that under physical conditions corresponding to those in the experiment, three stages of acceleration, namely, the TNSA, RPA and RITA stages, can be distinguished. In such conditions, the generation of a quasi-monoenergetic spectral peak seems to be the result of the appropriate relationship between the durations of the RPA and RITA stages. Based on the simulations performed, it has also been found that at very high intensities (up to >10^{22} W/cm^2) achievable with multi-PW lasers, the generation of heavy ion beams with a narrow energy spectrum is also possible provided that an appropriate control of the laser pulse duration is ensured and the duration is well matched to the target thickness.

Table 3 summarises the results of measurements of the maximum charge states and maximum energies of heavy ions forward accelerated by short (fs or sub-ps) laser pulses with relativistic intensity in the range from ~10^{20} W/cm^2 to ~10^{22} W/cm^2. As expected, the Z_{max} values increase with the increasing atomic/mass number of the ion and are the highest for Au ions (Z_a = 79) for which they reach up to Z_{max} = 72. In the studied cases, ionisation of target atoms was usually the result of a combination of collisional ionisation with field ionisation; therefore, Z_{max} depends not only on the laser intensity, I_L, but also on the laser pulse duration, τ_L, and the target thickness, L_T (an increase in τ_L and L_T can increase the number of electron–ion collisions and lead to an increase in the ionisation probability). The maximum ion energies achieved in the considered laser intensity range reach up to ~2 GeV. They depend on I_L, but the key parameter determining these energies seems to be the laser fluence $F_L = I_L\tau_L$. The maximum ion energy depends of course on the target thickness. Reducing L_T favours increasing E_{max}, but usually leads to a decrease in the number of generated ions. Therefore, obtaining the desired values of Z_{max} and E_{max} requires an optimal balance between at least three parameters of the laser-target system: I_L, F_L (or τ_L) and L_T.

Table 3. Maximum charge states, Z_{max}, and maximum energies, E_{max}, of heavy ions accelerated forward by an ultrafast laser. I_L, τ_L, and E_L are the intensity, duration, and energy of the laser pulse, respectively.

Element	Z_{max}	E_{max}, GeV	I_L, 10^{20} W/cm^2	τ_L, fs	E_L, J	References
$^{56}Fe^{26}$	~25	0.9	10	35	8	[92]
$^{108}Ag^{47}$	45	≥2.2	50	40	12	[95]
$^{197}Au^{79}$	56	0.2	0.8	35	1.3	[93]
$^{197}Au^{79}$	~50	≥1	8	140	~100	[94]
$^{197}Au^{79}$	61	1.1	110	22	15	[12]
$^{197}Au^{79}$	72	≥1.4	4	500	185	[96]
$^{197}Au^{79}$	58	1.6	3–5	850	200	[98]
$^{197}Au^{79}$	51	2	3	800	175	[99]

In parallel with the experimental research, theoretical studies on laser-driven heavy ion acceleration were conducted, based primarily on numerical simulations using particle-in-cell (PIC) codes [69,74,75,99–107]. Usually, two-dimensional (2D PIC) codes were applied, and sometimes one-dimensional (1D PIC) and three-dimensional (3D PIC) codes were used. Numerical simulations were performed for relativistic laser intensities in the range from ~10^{20} W/cm^2 to ~10^{22} W/cm^2, achievable by ultrafast lasers in the last decade, and laser pulse durations from ~30 fs to 600 fs. The acceleration of super-heavy ions (Au) was most often studied [69,74,75,99,103,105–107], but also the acceleration of heavy ions with lower mass numbers such as Fe ions [100–102] or Cu ions [104] was investigated. In the simulations, targets of various thicknesses and structures were used, starting from sub-micrometre flat single-layer targets (with thicknesses from 10 nm to 500 nm) [69,99,101,104–106] to double-layer [74,75,102,104,107] and multi-layer [100] targets comprising layers with different atomic numbers. The studies carried out covered a very wide range of issues and concerned, in particular, acceleration mechanisms (e.g., identification of conditions for the occurrence/dominance of the RPA, TNSA, RITA or CEA mechanism [69,75]), mechanisms of ionisation of target atoms and accelerated ions [104–106], properties of generated ion beams and their dependence on laser parameters (e.g., intensity or duration of the laser pulse [69,75,105]) and/or target parameters [104,106,107], and many other issues. These studies enabled a fairly comprehensive understanding of the heavy ion acceleration process in the studied range of laser intensities, improved theoretical models of this process, and opened the way to improving the parameters and quality of generated heavy ion beams.

In summary, the increase in the peak power of ultrafast lasers from the TW level to the PW level observed in the last two decades and the accompanying increase in laser intensity by several orders of magnitude, up to the level of 10^{22} W/cm^2, resulted in the increase in the energy of accelerated heavy ions from ~1 MeV to ~1 GeV, as well as a significant increase in other ion beam parameters such as beam intensity and fluence or the number of generated multi-charge high-energy ions. Theoretical and numerical studies on laser-driven heavy ion acceleration conducted during this period significantly expanded our knowledge of this process, helped explain and interpret measurement results, and pointed the way towards further improvement of in the parameters of generated heavy ion beams.

4. Acceleration of Heavy Ions at Ultra-High Laser Intensities

The results of the studies summarised in Section 3 have shown that at laser intensities in the range of 10^{20}–10^{22} W/cm^2, it is possible to produce heavy ions, including super-

heavy ions, with energies of ~1 GeV. However, for most of the potential applications of heavy ions in such domains as nuclear physics, particle physics, HEDP or ICF, ion energies of multi-GeV and higher, up to ~TeV, are required. Achieving such ion energies seems possible at ultra-high intensities of ~10^{23}–10^{24} W/cm^2 or higher. Recently constructed multi-PW femtosecond lasers [10–13] enabling the generation of ultra-high laser intensities of ~10^{23} W/cm^2 [13] and designed fs lasers with pulse powers up to 100 PW and laser intensities of ~10^{24} W/cm^2 [10,14–16] allow us to believe that laser-driven acceleration of heavy ions, including super-heavy ions, to energies of tens or even hundreds of GeV is feasible and will be experimentally demonstrated in the near future. The production of ion beams with such ion energies and other beam parameters enabling their effective use in various possible applications requires comprehensive studies, both experimental, theoretical and numerical. Although laser intensities of 10^{23} W/cm^2 have already been demonstrated [13], experimental studies on the acceleration of heavy ions at such intensities and higher are still at the design stage. Currently, only theoretical and numerical studies of heavy ion acceleration at ultra-high laser intensities are possible. It can be believed that they will allow for the understanding of the acceleration mechanisms and properties of heavy ion beams generated at such intensities, will be helpful in the design and preparation of appropriate experiments, and will outline the perspectives of various applications of such beams.

These studies are currently being developed, but are still at a very early stage [5,64,65,108–112]. They require advanced numerical tools, including PIC codes that take into account physical phenomena that do not occur at lower laser intensities, such as, for example, radiative losses due to the emission of synchrotron radiation by ultra-relativistic electrons produced by the laser [113–118] and, at intensities approaching 10^{24} W/cm^2, also quantum effects (e.g., production of electron–positron pairs and a cascade of other phenomena) [108,112,114,115,117,118].

In this section, we will present selected results of numerical studies of heavy ion acceleration at laser intensities of ~10^{23} W/cm^2 performed recently by the authors of this article. The numerical simulations underlying this study were performed using the multi-dimensional (2D3V) PICDOM code [119], which takes into account, in particular, the dynamic ionisation of target atoms and accelerated ions, as well as the radiation losses induced by the synchrotron radiation emission. Most of the results of this study have not been published so far. In Section 4.1, we present the results of studies on the acceleration of super-heavy ions driven by a multi-PW femtosecond laser pulse, while in Section 4.2, we show some results obtained for heavy ion beams accelerated by a high-energy (>100 kJ) picosecond laser pulse, made with the aim of using such beams in inertial confinement thermonuclear fusion.

4.1. Acceleration of Super-Heavy Ions by a Multi-Petawatt Femtosecond Laser

The results of studies discussed in this sub-section are based on PIC simulations of the acceleration of super-heavy ions generated from ultra-thin ($\leq$100 nm) solid-state-density Au, Pb, Bi or U targets irradiated by a 30-fs circularly polarised laser pulse with a wavelength of 0.8 μm, a beam width (FWHM) d_L = 3 μm, and a peak intensity from 5 × 10^{22} W/cm^2 to 2 × 10^{23} W/cm^2. Such laser pulse parameters are expected to be achieved in ultrafast multi-PW lasers already in operation or under construction [10–13]. It was assumed that the targets have the same areal mass density equal to $\sigma = \rho L_T$ =1.36 g/m^2, where ρ is the mass density and L_T is the thickness of the target (this areal mass density corresponds to the thicknesses of the Au, Pb, Bi, and U targets of 50.5 nm, 100 nm, 119 nm, and 51.4 nm, respectively). More details about the simulation parameters can be found in [65].

As already stated in Section 3, the efficiency of heavy ion acceleration strongly depends on the ratio of the charge state of the ion to its atomic mass, i.e., the Z/A ratio. Achieving high values of this ratio enabling highly effective acceleration of super-heavy ions, therefore requires achieving very high values of the charge state Z, which is not easy due to the high ionisation potentials of such ions. In the acceleration of super-heavy ions, ionisation processes play a much more important role than in the case of light ions for which, due to relatively low ionisation potentials, achieving high values of the Z/A ratio is much easier. In particular, light ions completely devoid of electrons can be obtained at relatively low laser intensities of ~10^{20}–10^{21} W/cm^2 and ionisation of the (ultra-thin) target occurs almost instantaneously (usually within a few fs). Therefore, in the case of light ions, we usually deal with the acceleration of one type of ion with a charge state Z = $Z_a \approx 1/2$ A (Z_a is the atomic number of the target atom). In the case of super-heavy ions/atoms, even at ultra-high intensities $\geq 10^{23}$ W/cm^2, achieving full ionisation of the atom (ions completely stripped of electrons) is usually not possible, the target ionisation is not instantaneous (it lasts at least several dozen fs), and the generated plasma is a collection of many types of ions with various charge states. Although at ultra-high laser intensities the process of ionisation of atoms and ions seems less complex than for lower intensities ($<<10^{23}$ W/cm^2), because only one type of ionisation—field ionisation—occurs (impact ionisation is negligible), the ionisation spectrum of super-heavy ions is usually very complex. Knowledge of the properties of this spectrum is therefore essential for understanding the acceleration process of such ions and its possible optimisation.

Figure 4 presents the ionisation spectrum of Au, Pb, Bi, and U ions in the final stage of ion acceleration by a 30-fs laser pulse with an intensity of $I_L = 10^{23}$ W/cm^2. As can be seen, the structure of the ionisation spectrum in the final acceleration stage for all the super-heavy ions studied is fairly similar. In each of the cases considered, a large number of ion species with different charge states are produced, but in each case the spectrum is dominated by Ne-like ions and Ni-like ions. The relatively high populations of Pd-like, Ni-like, and Ne-like ions in spectra in the Figure can be a result of the fact that the remaining completely filled d^{10} shells or p^6 shells of Ne-like ions are relatively stable, i.e., the energy of electron detachment from such a shell is much greater than the energy of detachment from unfilled shells. As shown in [65], Ne-like ions are actually created only by the laser field in the RPA acceleration stage, while ions with lower charge states are created by both the laser field and the TNSA-like field induced in the plasma by relativistic laser-generated electrons. Both the average charge state Z_{mean} of the ions and the absolute value of the charge state of the Ne-like ions increase with the increasing atomic number of the target Z_a. With the increasing Z_a, the ratio of the population of Ne-like ions to the population of Ni-like ions also increases and in the case of uranium, the population of Ne-like ions clearly dominate the population of other ion types. Except for a small number of ions with a charge state higher than that of the Ne-like ions, the latter have the highest Z/A ratio and thus their acceleration efficiency should be the highest (see below).

Two-dimensional (2D) distributions of charge state and density of Au, Pb, Bi, and U ions are presented in Figure 5. The charge state distributions of Au, Pb, Bi, and U ions are similar. Low-energy ions, concentrated close to the initial target position (x = 1 μm) have low charge states, while high-energy ions are highly charged ions with very similar charge states (for these ions practically one colour dominates in each of the four presented distributions). As a more detailed analysis shows, the high-energy ions, especially those propagating near the laser axis (y = 0) are dominated by Ne-like ions with charge state 69 for Au, 72 for Pb, 73 for Bi, and 82 for U. The 2D density distributions of Au, Pb, Bi, and U ions are also similar to each other and their shape largely reproduces the shape of the ion charge state distributions. As it results from the analysis of acceleration stages earlier

than those in Figure 5, in the first stage of acceleration, lasting for a period close to the laser pulse duration, the RPA mechanism dominates—first RPA-HB and then RPA-LS. In this stage, a dense bunch of high-energy highly charged ions is formed, which propagates forward near the laser axis. In the post-RPA stage, ions are accelerated mainly by the TNSA mechanism. This mechanism leads not only to an increase in ion energy, but also to a broadening of the ion energy spectrum. In the post-RPA stage, the CEA (Coulomb explosion acceleration) mechanism also has a significant influence on the properties of the ion beam. CEA accelerates ions in all directions, especially in directions transverse to the beam axis, which results in the scattering of a significant part of ions into a large solid angle (this can be seen in Figure 5) and an increase in the angular divergence of the ion beam, as well as a broadening of its energy spectrum. As a result of the destructive influence of CEA on the generated ion beam (and partly TNSA and plasma instabilities), only the paraxial part of the ion beam has a relatively small angular divergence (see below) enabling its propagation over distances significantly exceeding the size of the ion source without a dramatic decrease in ion density. Moreover, in this part of the beam, ions with the highest energy and the highest charge state are accumulated. This allows us to assume that the paraxial part of the beam is the most useful from the point of view of potential applications of laser-accelerated super-heavy ions.

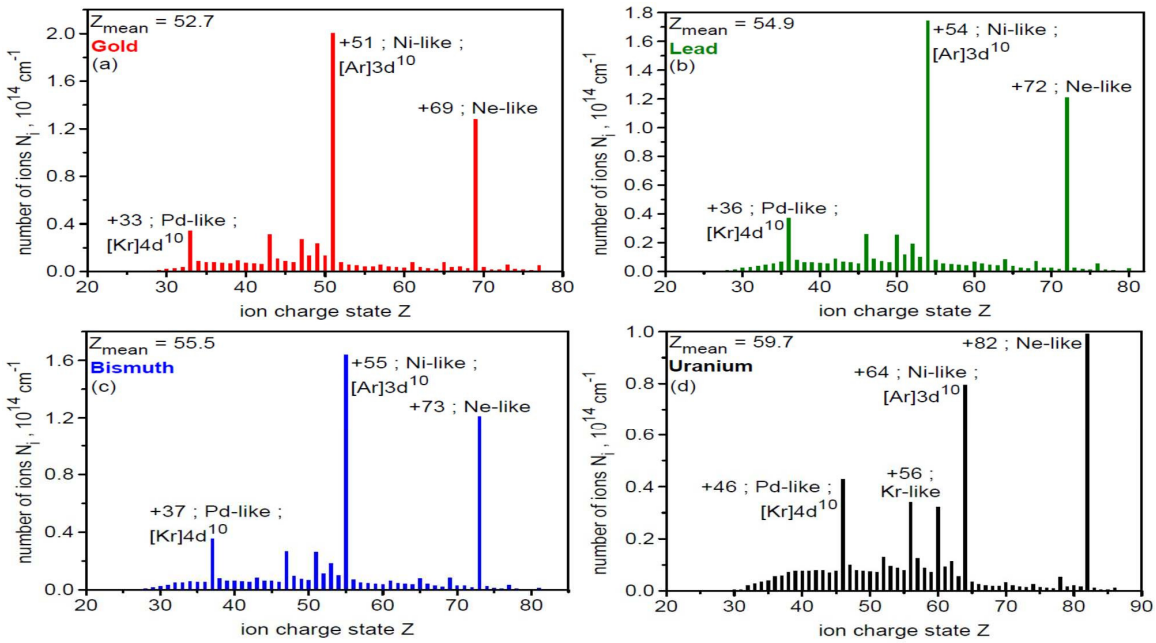

Figure 4. The ionisation spectra of Au, Pb, Bi, and U ions in the final stage of ion acceleration. $I_L = 10^{23}$ W/cm^2.

Since the properties of the ion beams illustrated in Figures 4 and 5 and described above are qualitatively very similar for Au, Pb, Bi, and U ions, we will demonstrate other properties of the super-heavy ions only for one of the considered ion types, namely, Au ions.

Figure 6 shows the energy spectra of Au ions for Ne-like ions and several other high-charge, high-energy ion species for the whole ion beam (a) and for the paraxial beam (b). The paraxial beam was selected from the whole gold ion beam by a 5-μm diaphragm placed on the axis (y = ±2.5 μm) at a distance of x = 30 μm from the target. It can be seen that for both the whole ion beam and the paraxial beam the high-energy part of the spectrum extending from ~2 GeV to ~60 GeV is dominated by Ne-like ions, while the contribution of

the other ion species to this part of the spectrum for the paraxial beam is clearly smaller than for the whole beam.

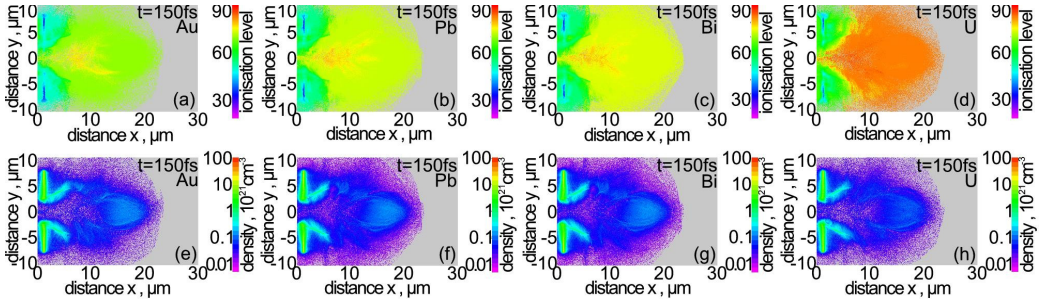

Figure 5. The 2D spatial distributions of the charge state (**a**–**d**) and the ion density (**e**–**h**) of Au, Pb, Bi, and U ions in the final stage (150 fs) of ion acceleration driven by a 30-fs laser pulse of intensity $I_L = 10^{23}$ W/cm^2. The colours in sub-Figure a–d correspond to charge states (ionisation levels) with Z values presented on the linear colour scale on the right side of each sub-Figure. The colours in the sub-Figure e–h correspond to the ion densities (in units of 10^{21} cm^{-3}) presented on the logarithmic colour scale on the right side of the sub-Figure.

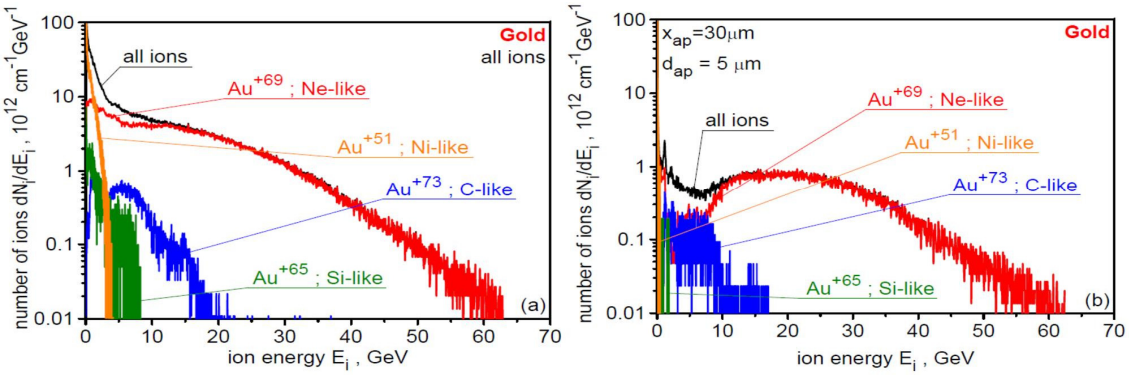

Figure 6. The energy spectra of Au ions recorded at the end of simulation (t = 240 fs): (**a**) for all ions (black curves) and ions with high energies and high Z; (**b**) for all ions in the paraxial beam (black curves) and ions with high energies and high Z in the beam. The paraxial beam was selected from the whole gold ion beam by a 5-μm diaphragm placed on the axis (y = ±2.5 um) at a distance x = 30 μm from the target. $I_L = 10^{23}$ W/cm^2.

The dominance of Ne-like ions (Z = 69) in the generated Au ion beam is even better seen in Figure 7, which shows the numerical values of the total energy carried by Au ions with charge state Z (a) as well as the mean (b) and maximum (c) energies of these ions for the whole ion beam (green) and the paraxial beam (red). In the case of the whole beam, Ne-like ions carry 90% of the beam energy, while in the case of .the paraxial beam, the energy stored in Ne-like ions exceeds 95% of the (paraxial) beam energy. Moreover, in both cases, the mean and maximum energy of Ne-like ions is much higher than those of the other ion species. We can therefore state that the generated Au ion beam, especially the paraxial beam, is actually a mono-charge beam. As shown in [64,65], the dominance of Ne-like ions in beams of super-heavy ions accelerated by an ultra-high intensity laser pulse is an inherent feature of these beams in a rather wide range of intensities around 10^{23} W/cm^2, resulting from the matching of the laser intensity to the energy level structure of super-heavy ions.

Significant differences between the characteristics of the whole generated Au ion beam and its paraxial part, which largely determine the usefulness of the ion beam in possible applications, are especially clearly visible in the angular distributions of mean ion energy and ion energy fluence $F_i = \sigma_i E_i$. This is illustrated in Figure 8. As can be seen, the angular

distributions of both ion fluence and mean ion energy for the whole beam are much wider than for the paraxial beam. This is the result, on the one hand, of the contribution to the acceleration process of the CEA mechanism pushing ions in directions transverse to the beam axis, and on the other hand, of the inhomogeneity of the spatial distribution of the laser beam intensity, which causes the generation (on the slopes of the distribution) of ponderomotive forces directed transverse to the beam axis and accelerating electrons and ions at a large angle to the axis.

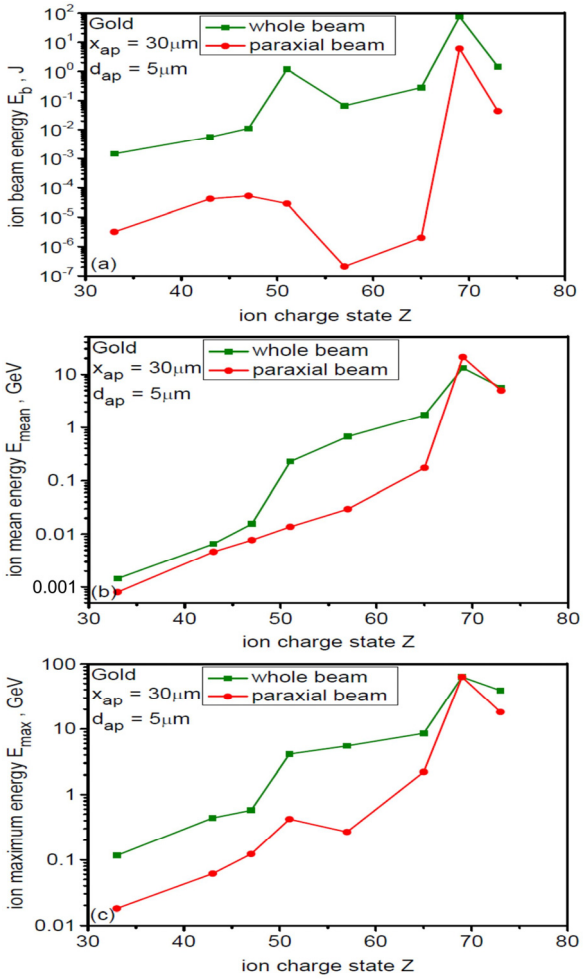

Figure 7. The total energy carried by Au ions with charge state Z (**a**) as well as the mean (**b**) and maximum (**c**) energies of these ions for the whole ion beam (green) and the paraxial beam (red). $I_L = 10^{23}$ W/cm^2.

The angular divergence of the paraxial beam (measured by the width of the angular distribution of the fluence or energy of ions) increases with the increasing width of the beam-limiting aperture, d_{ap}. It is obvious that with the increase in d_{ap} the beam energy E_b and the number of ions N_i in the beam will increase. However, the utility of the ion beam is determined not only by E_b and N_i, but also by many other beam parameters that can be controlled by changing the d_{ap}. Figure 9 shows the dependence of Ni and the ion beam energy fluence (averaged over the aperture area), F_b, in the Au ion beam on the aperture width d_{ap}. As can be seen, although the number of ions increases with the increase in the aperture size, the ion beam energy fluence F_b decreases with the increase in d_{ap} and is the highest for the paraxial beam. This is because the average ion energy takes the highest values in the paraxial region. Thus, although the total ion energy and the number of ions in the whole beam are higher than for the paraxial beam, other beam parameters that

determine its usability, such as the mean and maximum ion energy and the beam intensity and fluence, are clearly higher for the paraxial beam.

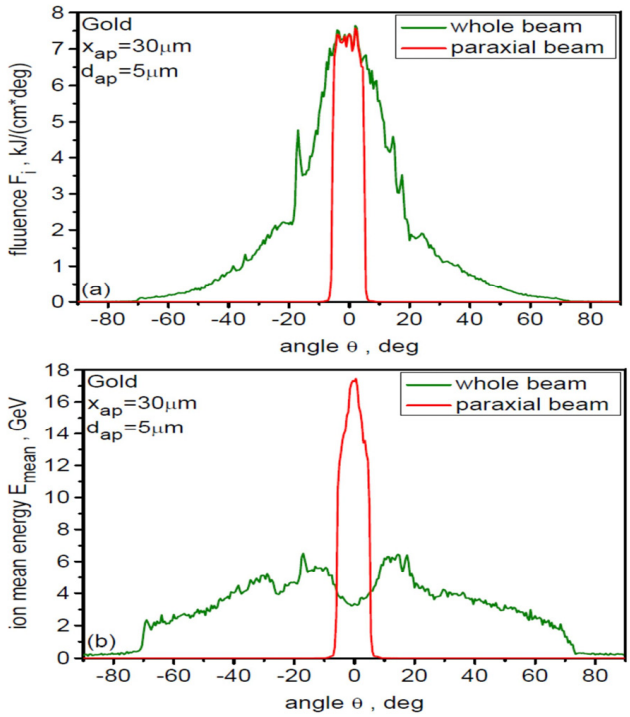

Figure 8. The angular distributions of energy fluence (**a**) and mean energy (**b**) of Au ions for the whole beam (green) and the paraxial beam (red). $I_L = 10^{23}$ W/cm^2.

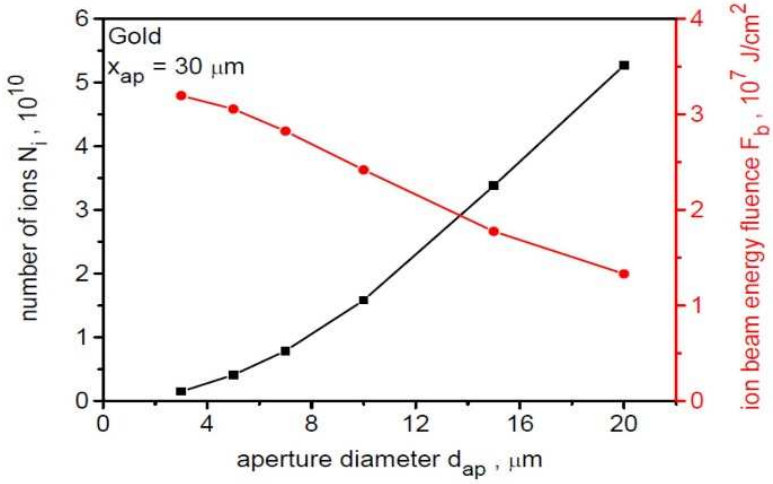

Figure 9. The total number of ions N_i and the ion beam energy fluence (averaged over the aperture area) in the Au ion beam as a function of the beam-limiting aperture width d_{ap}. $I_L = 10^{23}$ W/cm^2.

It can be expected that with the increase in the laser pulse intensity, I_L, the energy of Ne-like ions, dominating in the ion beam and determining its main parameters, will increase. However, since the number of generated Ne-like ions depends on the degree of matching of the laser intensity to the structure of energy levels of gold atoms, it is not clear whether other parameters characterising the beam, in particular, the total energy carried by Ne-like ions, E_b, and the efficiency of conversion of laser energy to Ne-like ions, η, will also increase with the increase in I_L. The answer to this question can be found in Figures 10 and 11, which show the dependence of E_{mean} and E_{max} as well as E_b and η on the laser intensity I_L for the whole Au ion beam and the paraxial beam.

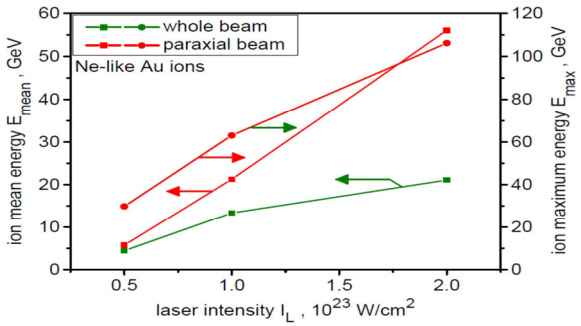

Figure 10. The dependence of the mean and maximum energy of Ne-like Au ions on the laser intensity for the whole beam (green) and the paraxial beam (red). The arrows point to the axis to which the given relationship applies.

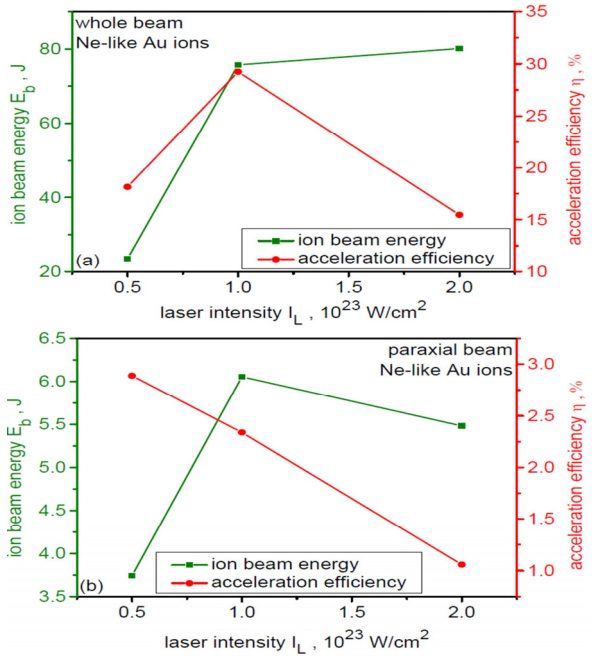

Figure 11. The dependence of the Ne-like ions total energy and the laser-to-Ne-like ions energy conversion efficiency for the whole beam (**a**) and the paraxial beam (**b**).

As expected, the mean and maximum energy of Ne-like ions increases with increasing laser intensity for both the whole beam and the paraxial beam. However, the dependence of the efficiency of laser energy conversion into Ne-like ion energy η is more complex. For the whole beam, this dependence has a non-monotonic course with a maximum near $I_L = 10^{23}$ W/cm^2, while in the case of the paraxial beam, the conversion efficiency decreases with the increasing I_L. This results from the fact that the optimal laser intensity ensuring the maximum efficiency of ionisation of gold atoms to the charge state corresponding to Ne-like ions lies in the intensity range of (3.3–8.9) × 10^{22} W/cm^2 [65], i.e., close to the lowest I_L value assumed in the simulations whose results are presented in Figures 10 and 11.

In summary, the results presented in this sub-section have shown that the dominant mechanism of acceleration of super-heavy ions from sub-micrometre targets at ultra-high laser intensities is RPA, but TNSA and CEA also have a noticeable effect on the final parameters of the ion beam. Although TNSA and CEA mechanisms increase the ion energy achieved in the RPA acceleration stage, they also lead to an increase in the beam angular divergence and a broadening of its energy spectrum. In the RPA stage, the target atoms and then the resulting ions are ionised by the laser field, while in the post-RPA stage, additionally by the field induced in the plasma by high-energy electrons generated by the

laser. Despite the fact that many ion species with different charge states are created in the ionisation process, at laser intensities of ~10^{23} W/cm^2, the vast majority of the beam energy is carried by Ne-like ions (e.g., for Au Z = 69), which also have much higher mean and maximum energies than the other ion species. This mono-chargeability of super-heavy ion beams is an inherent feature of these beams resulting from matching the laser intensity to the energy level structure of super-heavy atoms. The efficiency of laser energy transformation into the energy of a super-heavy ion beam accelerated by a femtosecond pulse of ultra-high intensity is very high and can exceed 30%. However, for potential applications, the paraxial part of the beam seems to be the most useful. The paraxial beam is actually a mono-charge beam (Ne-like ions carry over 95% of the beam energy), and has a small angular divergence enabling its practical use at large distances from the target.

4.2. Acceleration of Heavy Ions by a High-Energy Picosecond Laser

As shown in Section 4.1, using multi-PW lasers generating femtosecond pulses with ultra-high intensity of ~10^{23} W/cm^2, it is possible to produce heavy ion beams with ion energies of ~100 GeV and ion beam energies E_b approaching 100 J. However, some potential applications of laser-accelerated heavy ion beams require much higher parameters than those achievable using femtosecond lasers. These include inertial confinement (thermonuclear) fusion (ICF) in the so-called ion fast ignition (IFI) option, in which a nuclear fuel (usually deuterium-tritium—DT) compressed to high densities is ignited by an intense ion beam [120–128]. Achieving fuel ignition in the IFI option of ICF requires a picosecond ion beam (light or heavy ions) with extremely high parameters, in particular, the beam energy E_b > 10 kJ and the beam intensity I_b~10^{20} W/cm^2 [127–130]. Moreover, the mean ion energy in the quasi-monoenergetic energy spectrum should be well matched to the fuel density, and in the case of heavy ions, it should usually be of the order of 100 MeV/u [127–131]. Achieving such beam parameters in conventional RF accelerators in the foreseeable future is rather unlikely, but it seems possible using picosecond lasers with very high energy above 100 kJ. The possibility of achieving the beam parameters required for IFI by heavy ion beams driven by a picosecond laser with energy of 150–250 kJ was investigated by the authors of this paper and presented in [66]. Example results of these studies, obtained from simulations using the PICDOM code, are shown in Figures 12 and 13. They illustrate how the ion beam parameters crucial for thermonuclear ignition depend on the atomic number of the ion accelerated by a picosecond laser with energy of 200 kJ. The comparison presented in these Figures was made for ions produced from Al, Ti, Cu, Ag, and Au targets with the same areal mass density $\sigma = \rho L_T$ = 2.2 mg/cm^2.

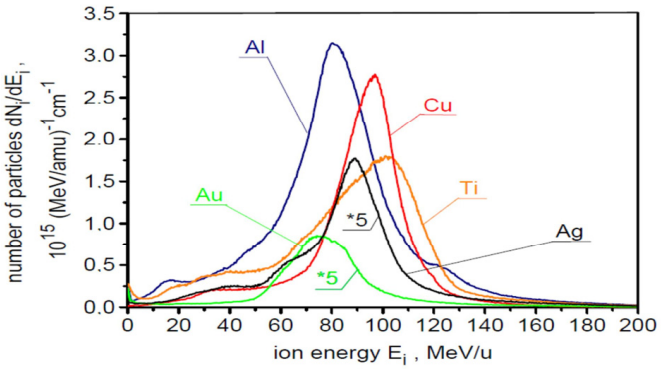

Figure 12. Energy spectra of Al, Ti, Cu, Ag, and Au ions accelerated by a 1-ps laser pulse with an intensity of 5.2 × 10^{22} W/cm^2 and energy of 200 kJ for a paraxial ion beam limited by a 50-μm aperture corresponding to the size of the compressed DT nuclear fuel. Dependencies for Au and Ag have been multiplied by 5 for better visualization.

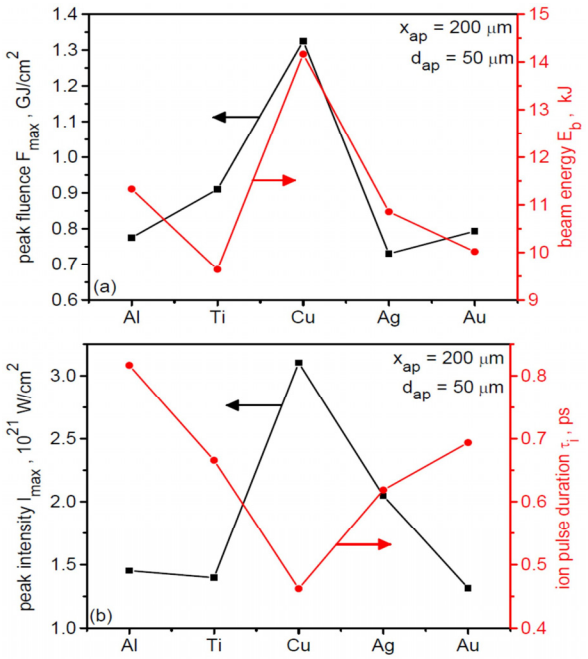

Figure 13. The peak fluence and energy (**a**) as well as peak intensity and duration (**b**) of the Al, Ti, Cu, Ag, and Au ion beams produced by a 1-ps laser pulse with an intensity of 5.2 × 10^{22} W/cm^2 and energy of 200 kJ for a paraxial ion beam limited by a 50-μm aperture corresponding to the size of the compressed DT nuclear fuel.

As can be seen from Figure 12, for all considered ion types, it is possible to produce an ion beam with a quasi-monoenergetic spectrum; however, the width of the spectrum and the mean energy of the ions, E_{mean}, depend on the type of ion. The narrowest spectrum and the highest E_{mean} value of ~100 MeV/u are found for Cu ions. The observed differences in the energy spectra of the considered ion types result from differences in the Z/A ratio for these ions, as well as from certain differences in the acceleration mechanisms of these ions [66].

The dependence of the parameters determining the possibility of thermonuclear ignition in the IFI option, i.e., the peak fluence and energy of the ion beam, as well as the peak intensity and duration of the beam, on the type of accelerated ion is presented in Figure 13. As can be seen, the highest values of fluence, energy and intensity of the ion beam and the shortest ion pulse duration are obtained for Cu ions. Moreover, in the case of the Cu ion beam, the absolute values of these parameters meet the IFI requirements for the conditions considered, while for the remaining ion types only some of these requirements are met.

The presented results prove that for fixed laser parameters (energy, power, and intensity) it is possible to identify the type of ion with the optimal mass number A ensuring the achievement of the highest values of ion beam parameters determining thermonuclear ignition. It should be noted, however, that for a given laser power and energy, changing the laser beam intensity (e.g., by changing the laser focal spot size on the target) can lead to a change in the optimal ion mass. It can be expected that increasing the laser intensity will result in a shift of the optimal ion mass towards higher values of A, while decreasing the intensity will lead to a shift of the optimal mass towards lower values of A.

In conclusion, the studies conducted by the authors of this article—the example results of which are presented above—have shown that achieving thermonuclear ignition of DT fuel by a heavy ion beam is basically possible with realistic laser and fusion target parameters.

4.3. Discussion

As is well known, when the parameter $\chi_e \approx 0.09 I_L[10^{23}\ W/cm^2]\lambda[\mu m]$ is ~1 or higher quantum effects in laser–matter interaction become important [132,133]. In the known numerical studies of heavy ion acceleration in which some quantum effects were included in the 2D PIC code, the laser intensity was $<10^{24}$ W/cm^2, and the values of χ_e were ~0.3 [110,112] or <0.8 [111]. However, in these works, no significant influence of quantum effects included in the simulation on the parameters of the ion beam (Au ions) was found. In our studies presented in this article (Section 4), the values of the parameter X were as follows: for laser fs pulses (Section 4.1) $\chi_e \leq 0.15$ (in most cases $\chi_e \approx 0.07$) and for ps pulses (Section 4.2) $\chi_e \leq 0.04$. Moreover, both fs and ps laser beams had circular polarisation for which the efficiency of generation of relativistic electrons is lower than for linear polarisation [1,2] and the probability of quantum effects occurrence is lower, especially when the ion acceleration process is dominated by the RPA-LS mechanism [117,118]. The influence of quantum effects in the cases studied by us could therefore be neglected.

Despite the "non-quantum" nature of laser–plasma interaction, the emission ("classical") short-wavelength synchrotron radiation (Gamma radiation) by relativistic electrons due to radiation friction forces [113–118] was significant. It was found that the efficiency of laser energy transfer to synchrotron radiation depends not only on the laser intensity, but also quite strongly on the laser pulse duration. For 30-fs pulses with an intensity of 10^{23} W/cm^2, this efficiency was ~several percent, while for a 1-ps pulse with twice lower intensity it reached several dozen percent (~20–30% for heavy ions and ~30–40% for light ions) [128,134,135]. As shown in our works [134,135], the radiation is emitted primarily from the plasma region in which the laser field (both incident and reflected from the critical plasma surface) interacts with relativistic electrons accelerated by laser-induced ponderomotive forces. The most intense radiation emission takes place in the skin layers of the plasma located near the central region of the laser beam, where the laser field strength is the highest. In these plasma regions, the radiation power density is extremely high and for a 1-ps laser pulse with an intensity of ~5×10^{22} W/cm^2 reaches values of ~10^{25}–10^{26} W/cm^3. The duration of the synchrotron radiation pulse is close to the duration of the laser pulse, and thus the power of this radiation is very high. At a 1-ps pulse energy of 200 kJ, the peak power and energy of radiation emitted from a low-Z target (e.g., C target) can reach ~70 PW and ~60 kJ, respectively [134,135]. With the increase in the atomic number of the target, the laser-radiation energy transfer efficiency decreases and for heavy ions it is by a factor of $\geq$1.5 lower than for light ions [135], but still the radiation pulses from high-Z targets have very high power and energy reaching tens of PW and tens of kJ [135].

Radiational losses associated with the emission of Gamma radiation accompanying ion acceleration at ultra-high laser intensities lead to a decrease in the values of practically all important parameters of the generated ion beam (maximum and mean ion energy, intensity, fluence and energy of the ion beam, etc.). In the case of laser-driven ion accelerators intended for thermonuclear fusion (Section 4.2), the decrease in ion beam parameters caused by these losses can reach several dozen percent [128,134,135]. In addition, powerful Gamma radiation pulses can pose a serious threat to the fusion facility infrastructure. From this point of view, the emission of this radiation during ion acceleration is a parasitic phenomenon. On the other hand, the controlled generation of multi-PW pico- or sub-picosecond Gamma-ray pulses from a laser accelerator can be used in new research areas and applications difficult to explore with the current Gamma-ray sources.

5. Challenges Facing Research on Laser-Driven Ion Acceleration

Despite the significant progress in the laser-driven heavy ion acceleration research over the past two decades, this research can still be considered to be in its early stages. There are many challenges ahead of this research, both cognitive and technological, especially when viewed from the perspective of potential applications of future laser-driven ion accelerators. Below we outline the more important of these challenges.

5.1. Control of the Ionisation Spectrum and Generation of Mono-Charge Beams

As shown earlier in this article, unlike a beam of light ions, a beam of laser-accelerated heavy ions contains a large number of ion species with different values of the charge state to ion mass ratio Z/A. Since this ratio determines the efficiency of ion acceleration by laser-induced electric fields in the plasma and is distributed heterogeneously in the plasma, this multi-charge of the ion beam is one of the most important, inherent properties of the heavy ion beam, which determines to a large extent other beam characteristics such as the energy spectrum of accelerated ions, the beam angular divergence, the degree of spatial homogeneity of the beam parameters (ion energy, beam fluence, and intensity) or the energy efficiency of beam acceleration. For this reason, the key challenge for heavy ion acceleration is to find ways to control the beam ionisation spectrum. The discovery of the possibility of generating a mono-charge beam of super-heavy ions by matching the laser intensity to the energy level structure of the ion/atom at ultra-high intensities [64,65] is an important step forward towards controlling the ionisation spectrum of heavy ions. However, further progress is needed in this matter, in particular, finding ways to control this spectrum for various types of ions and different laser beam parameters is still an important and current research task.

5.2. Generation of Ion Beams with a Narrow Energy Spectrum

In many potential applications of laser-accelerated heavy ion beams, a narrow energy spectrum of the ions is desirable. Unfortunately, the energy spectrum of heavy ions demonstrated in real or numerical experiments performed today is broad (usually $\Delta E/\langle E\rangle \sim 1$ or wider) at both moderate and high laser intensities. Basically, with the help of appropriate transport and selection systems, a part of this spectrum with a small width (e.g., $\Delta E/\langle E\rangle \sim$ a few percent) can be separated; however, this is usually associated with huge beam energy losses, which may put in question the usefulness of the ion beam. The main reason for the broad spectrum of heavy ions, apart from the multi-charge of the ion beam mentioned above, is the complex process of heavy ion acceleration in which a significant role is usually played by no less than three acceleration mechanisms: RPA, TNSA, CEA (with a suitably thin target and/or a suitably long laser pulse, the RITA mechanism may also play an important role in this process). TNSA and CEA generally cause the broadening of the energy spectrum; therefore, minimising their contribution to the acceleration process may be a way to narrow the spectrum. Minimising the contribution of these two mechanisms may, however, be associated with a decrease in the maximum and mean ion energy and, consequently, with a decrease in other parameters such as beam intensity and fluence. Even if TNSA and CEA were eliminated from the acceleration process, the RPA acceleration is also not free from factors causing spectrum broadening such as non-uniform temporal and spatial distribution of laser beam intensity—resulting in a non-uniform distribution of ion velocities already at the initial stage of acceleration—or plasma instabilities (Raileigh-Taylor and others) developing during acceleration. Generating a beam of heavy ions with a narrow energy spectrum while maintaining the highest possible energy efficiency of acceleration is therefore a very difficult task waiting to be solved.

5.3. Acceleration of Heavy Ions to Teraelectronvolt Energies

Different potential applications of laser-driven heavy ions have different requirements for ion energy and the spectrum of desired ion energies ranges from sub-MeV to TeV. Experimentally measured energies of heavy ions (mainly Au ions) accelerated at laser intensities not exceeding 10^{22} W/cm^2 reach 2 GeV (see Table 3), while the maximum energies of super-heavy ions demonstrated in numerical simulations reach values of ~100 GeV at $I_L \approx 10^{23}$ W/cm^2 [65] and ~200 GeV at $I_L \approx 7 \times 10^{23}$ W/cm^2 [111]. Studies carried out so far show that a natural way to increase the ion energy is to increase the intensity and/or energy (actually fluence) of the laser pulse. The increase in ion energy is, however, limited by many factors, which are particularly evident in the case of relativistic ions and ultra-high laser intensities. One of the known and obvious factors in the case of relativistic ions is the increase in ion mass with the increase in its velocity (at the Au ion energy of 1 TeV, the ion mass is 6 times higher than its rest mass). Another factor that may play an important role in the acceleration of such ions is the limitation of ion velocity associated with the limited group velocity of the laser beam [136,137]. With the increase in I_L values in the region of ultra-high laser intensities $\gtrsim 10^{23}$ W/cm^2, "parasitic" phenomena limiting ion energy intensify. A particularly important "parasitic" phenomenon accompanying ion acceleration is the emission of electromagnetic radiation by relativistic electrons produced in laser–plasma interactions. It is the result of multi-photon Thomson and/or Compton scattering, in which an electron absorbs many photons from a laser beam and then scatters them into a single high-energy emitted photon. The value of the parameter $\chi_e \approx 0.09 I_L[10^{23}\ \mathrm{W/cm^2}]\lambda[\mu\mathrm{m}]$ [132,133] determines whether the radiation emission process is of classical or quantum nature. If $\chi_e \ll 1$, then the radiation emission process has a classical nature and is described by multi-photon Thomson scattering, while if $\chi_e \gtrsim 1$ ($I_L \gtrsim 1.1 \times 10^{24}$ W/cm^2 at $\lambda = 1$ μm), then the process has a quantum nature and is described by multi-photon Compton scattering. In the presence of a strong laser field, the high-energy photons produced in this process can produce electron–positron pairs by the Breit–Wheeler or the Trident process. The electrons and positrons produced in such a way can produce further photons by Compton scattering and further electron–positron pairs, leading to the formation of QED (quantum electrodynamic) cascades. The increase in laser intensity leads to the intensification of the above and other possible "parasitic" processes and at certain intensities the laser energy losses associated with these processes can be quite large that the ion acceleration process enters saturation. In the case of acceleration of heavy ions, the quantitative influence of "parasitic" processes occurring during the interaction of ultra-intense light with plasma on the ion acceleration is not known. It is therefore not known whether acceleration of heavy ions to TeV energies is feasible, and if that is the case, what are the physical conditions enabling the achievement of such ion energies. Clarifying the above issues and possibly developing an efficient method of accelerating ions to such energies seems to be one of the most serious scientific challenges facing laser-driven heavy ion acceleration.

5.4. Reducing the Ion Beam Angular Divergence

An important parameter of the ion beam, which largely determines its practical utility, is the angular divergence of the beam. The complexity of the heavy ion acceleration process and, in particular, the occurrence of several acceleration mechanisms and the variety of accelerated ion species, causes the angular divergence of the heavy ion beam to be generally large, usually much larger than in the case of light ions. Among several factors influencing the angular distribution of energy, fluence or intensity of generated ions, the most specific factor for heavy ions is the significant contribution to the acceleration process of the CEA mechanism. This mechanism accelerates ions in all directions, including

directions transverse to the laser beam axis. If at certain acceleration stages the CEA contribution becomes comparable to the RPA contribution, then a significant part of the ions is accelerated in directions transverse to the main ion propagation direction, which is usually the laser beam propagation direction. An important factor influencing the angular divergence of the ion beam is also the non-uniform spatial distribution of the laser beam intensity, which results in the generation of ponderomotive forces directed transverse to the beam axis and accelerating ions in non-axial directions. As shown in Section 4.1, the angular divergence of the heavy ion beam can be significantly reduced (from >60 degrees to ~10 degrees) by selecting from the whole beam its paraxial part with a transverse size comparable to the laser beam size. However, this is associated with a significant loss of the total ion energy, and thus a significant reduction in the efficiency of laser-to-ions energy conversion. Finding a way to produce a beam of heavy ions with a small angular divergence while maintaining high energy efficiency of acceleration remains an important problem waiting for an effective solution.

5.5. Increasing the Laser-to-Ions Energy Conversion Efficiency

An important parameter of a laser-driven accelerator, which largely determines the size and compactness of the accelerator, is the laser-to-ions energy conversion efficiency η. In heavy ion acceleration, the value of this parameter usually increases with the increasing laser intensity and at ultra-high intensities $\geq 10^{23}$ W/cm^2 can reach even several dozen percent [53]. Such high energy efficiencies of acceleration currently demonstrated in numerical experiments, however, refer to the whole generated ion beam (all accelerated ions), which at the current stage of research has relatively low quality (large angular divergence, wide energy spectrum). The development of methods for high-energy efficient generation of high-quality heavy ion beams is another practically important task requiring a solution.

5.6. Development of Numerical Tools

Laser-driven acceleration of heavy ions is a complex process, the detailed and comprehensive study and reliable description of which by analytical methods is not possible. Progress in the research of this process requires—apart from the development of experimental tools—further intensive development of numerical tools used in these studies. This concerns the development of multi-dimensional computer codes covering as many physical phenomena relevant to this process as possible (including quantum effects) and increasing computer power to be able to replace the currently commonly used two-dimensional codes with three-dimensional codes. It also seems necessary to increasingly include machine learning in these studies, which can be extremely useful in the search for the optimal set of laser and target parameters to achieve the desired characteristics of the ion beam.

5.7. Development of Ultrafast High-Peak-Power Laser Drivers

In order to achieve the research goals outlined above, it is necessary to develop the research infrastructure, first of all ultrafast high-peak-power laser drivers. Currently, there are several ultrafast lasers in operation in the world that generate laser pulses with a duration of several dozen fs, peak power in the range of 1–10 PW, and energy up to several hundred J [10–13]. The currently achieved intensities of focused beams of these lasers usually do not exceed 10^{22} W/cm^2 (in one of these lasers a higher intensity of 10^{23} W/cm^2 was measured [13]). However, the potential of these lasers is greater and by improving the quality of the laser beam and its focusing systems, it seems possible to achieve laser intensities of ~10^{23} W/cm^2. If the increase in laser pulse intensity was accompanied by an increase in its intensity contrast ratio, which would allow the use of ultrathin targets (<50 nm thick) in ion acceleration studies, it can be expected that the maximum energies

of generated heavy ions could reach several tens of GeV. However, a further increase in the energy of heavy ions, up to the sub-TeV range, requires a new generation of ultrafast lasers, i.e., lasers generating fs laser pulses with a power of ~100 PW, energy of ~several kJ, intensity of ~10^{24} W/cm^2, and intensity contrast ratio > 10^{13}. Although advanced projects of such lasers already exist [10,14–16], the construction of such research infrastructure will require a great scientific, technological, and financial effort and seems possible only in the next decade. As a device intended for fundamental/scientific research, such lasers do not require high repetition rates, and they do not necessarily have to meet other requirements specific to devices used for applications. However, a laser-driven heavy ion accelerator that could compete with conventional accelerators requires an even more complex laser infrastructure, in which a relatively compact laser driver with power $\geq$ 100 PW and multi-kJ energy operates with a high repetition rate (>>1 Hz). In addition, such a driver should provide high repeatability and flexibility of parameters and include many other features typical of conventional accelerators generating ion beams for various applications. The rational design and construction of such an accelerator will be possible only after gaining the necessary experience and knowledge from experimental devices currently being designed.

A separate and even more technologically demanding task is to design and build a laser driver generating ion beams for fast ignition of thermonuclear fusion, which—according to current knowledge—should generate laser pulses with a duration of 1–10 ps, power ~ 100 PW, and energy ~ 100–300 kJ. Such lasers require a different technology than femtosecond lasers and it will probably be a technology based in part on the experience of the technology for large high-energy lasers currently used in ICF research.

5.8. Development of Target Technology and Measurement Methods and Devices

The development of laser drivers should be accompanied by the development of technology for producing targets used in research on the laser acceleration of ions. Although the progress in this technology has been impressive in recent years (see e.g., [60]), new technological solutions that enable the optimal adjustment of target characteristics to laser parameters, especially in new ranges of laser intensities and energies following the development of laser drivers, are still desirable. These solutions should expand the range of available target thicknesses, densities and shapes, and enable the production of complex, multi-layer targets, including targets containing nano- or micro-layers with controlled density and spatial structure. Since more and more lasers used for ion acceleration will operate with a high repetition rate, the technology of targets designed for this type of lasers should be developed. In the longer term, this technology should ensure mass and possibly cheap production of such targets.

The development of research on laser acceleration of heavy ions also requires the development of methods and devices for diagnosing various parameters of generated ion beams. In particular, it is necessary to extend the range of measured ion energies (to the range of tens of GeV, and then sub-TeV and perhaps TeV range) and other parameters of the ion beam dependent on this energy. It is also highly desirable to increase the precision of measurements of various beam characteristics such as the ion energy spectrum, ionisation spectrum, spatial distribution of ion energy in the beam, etc. In the long term, these diagnostics should enable the measurement of parameters of ion beams generated with a high repetition rate.

6. Perspectives for the Application of Laser-Driven Heavy Ion Beams

The development of ultrafast high-peak-power lasers and the related progress in research on laser-driven heavy ion acceleration opens up the prospect of unique appli-

cations of heavy ion beams produced in laser accelerators in various domains. These include, in particular, nuclear and particle physics, high energy-density physics, inertial thermonuclear fusion, and materials science. Each of the above domains requires different ion beam parameters, the achievement of which requires overcoming different research and technological challenges.

6.1. Nuclear and Particle Physics

Short, pico- or sub-picosecond durations and extremely high intensities and densities of heavy ion beams driven by ultrafast high-peak-power lasers open up the prospect of research in nuclear and particle physics on new time scales and with ion beam–target interaction efficiency unattainable so far. In particular, some low-cross-section and/or transient nuclear reactions difficult to measure using ion beams produced by conventional accelerators could be possible to be studied. An example are the nuclear phenomena planned to be studied within the research program of the ELI-Nuclear Physics laser infrastructure, in which an ultrafast 10 PW laser would be used [138,139]. The aim of one of the topics in this program is to investigate the production of neutron-rich heavy nuclei by a new reaction mechanism called fission–fusion, using laser-accelerated thorium (^{232}Th) ion beams [138,139]. These studies are of high importance for nuclear astrophysics and their results could be a significant step towards understanding the nature of the creation of heavy elements in the universe. An experimental investigation of this problem using ion beams produced in conventional accelerators has not been possible so far because the required ion beam parameters were unattainable in these accelerators. In particular, the parameters of the thorium ion beam should be as follows: average ion energy ~1.6 GeV, ion number ~10^{11}, beam intensity and fluence 10^{20} W/cm^2 and ~10^{18} cm^{-2}, respectively. Numerical studies presented in [109,140] have shown that achieving such parameters is in principle possible with the intensity and power of the multi-fs laser pulse of ~10^{23} W/cm^2 and ~10 PW, respectively. Such laser pulse parameters are expected to be achieved in the ELI-Nuclear Physics infrastructure; however, to generate a thorium ion beam of sufficiently high quality required for conducting research on the production of neutron-rich heavy nuclei (a beam with a narrow energy spectrum and small angular divergence), a laser driver with higher parameters will probably be needed.

The increase in the energy of heavy ions to the level of ~1 GeV/u (i.e., energy ~ 200 GeV for A ~ 200) enables the study of quantum chromodynamic (QCD) effects such as the production of pions and kaons as well as equations of state for nuclear matter [141]. The possibility of producing gold ions of such energy at a laser intensity of ~7×10^{23} W/cm^2 was demonstrated in numerical simulations presented in [111]. Achieving such laser intensities seems possible using currently designed next-generation ultrafast lasers with power reaching ~ 100 PW. Further increase in the energy of laser-driven heavy ions up to ~1 TeV would enable a significant extension of QED studies and, in particular, the production of a highly exotic state of matter called quark-gluon plasma (QGP). The QGP is a state of matter consisting of an extended volume of interacting quarks, antiquarks, and gluons. Such a state of matter is thought to have existed a few microseconds after the Big Bang. The study of this new state will help to answer some of the key questions of nuclear and particle physics as well as the early evolution of the universe. The ion energy required to produce quark-gluon plasma decreases with an increasing ion mass number [110]; therefore, collisions of beams of super-heavy ions of appropriate energy and high intensity/fluence could be an effective source of QGP. Although laser-driven accelerators can potentially deliver heavy ion beams with intensities/fluences several orders of magnitude higher than conventional accelerators, achieving ion energies of ~1 TeV is an

open question, mainly due to the as yet unexplored influence of the "parasitic" phenomena (see Section 5) on the heavy ion acceleration process.

It can be believed that the development of laser-driven heavy ion accelerators, which in particular, will provide an extension of the range of achievable ion energies, will be accompanied by the expansion of research areas in nuclear and particle physics, in which laser-generated heavy ion beams can be effectively used.

6.2. High Energy-Density Physics

The high energy density (HED) state of matter is defined as a state in which the density of energy stored is higher than 0.1 MJ/cm^3 [142]. The production of HED states and the study of their properties are important for many fields of science, including thermonuclear fusion, astrophysics, planetary science, and materials science. Such states of matter can be produced by chemical explosions, lasers, Z-pinch devices and intense particle beams, including heavy ion beams [143,144]. The advantage of the latter is, in particular, the ability to create HED states basically in any dense material, deep penetration of the material, and usually quite good uniformity of the energy distribution deposited in the material.

The key parameters characterising the ability of the ion beam to create HED states are the energy deposited per gram of matter [144]: $E_s = (1.6 \times 10^{-19})(dE_i/dx)F_i$ [J/g] and the deposition power $P_s = E_s/t_d$, where dE_i/dx is the ion stopping power of the material, F_i is the ion fluence, and t_d is the energy deposition time. The estimates made in [4] showed that when a heavy ion (Pb) beam generated by an ultrafast multi-PW laser with an energy of ~200 J interacts with a carbon target, the E_s value reaches ~1 GJ/g while the value of P_s is above of 10^{20} W/g. For comparison, the E_s and P_s values predicted for heavy ion beams produced by very large RF-driven heavy ion accelerators, such as the FAIR accelerator (GSI, Darmstadt) or the HIAF accelerator (Institute of Modern Physics, Lanzhou), approach ~0.1 MJ/g and ~10^{12} W/g for FAIR and ~1 MJ/g and 10^{13} W/g for HIAF, respectively (assuming an energy deposition time of ~100 ns) [144]. Thus, the E_s and P_s values estimated for a multi-PW laser-driven heavy ion beam are many orders of magnitude higher than those achievable for some of the largest conventional accelerators. It should be emphasised, however, that the volume of matter in which the ion beam energy is deposited will be much smaller in the case of a laser-generated beam than for a beam from a conventional accelerator.

In addition to the very high intensity and density of laser-driven heavy ion beams, another important parameter that largely determines the nature of the beam–target interaction is the very short (ps or sub-ps) beam duration. This causes the time of energy deposition in the target to be much shorter than the period of time in which the target material parameters change due to its hydrodynamic motion. The interaction of the ion beam with the target is therefore isochoric in nature. Such an isochoric regime of beam–target interaction is difficult to achieve in the case of ion beams generated by conventional accelerators due to the long (ns or longer) durations of these beams.

The unique properties of laser-driven heavy ion beams, resulting in the extremely high values of deposited energy E_s and power P_s demonstrated in the above examples, as well as very short energy deposition times, open up the prospect of studying new regimes of ion–beam interaction with matter, unattainable or barely attainable for conventional accelerators.

6.3. Inertial Confinement Fusion

One of the important potential applications of laser-driven heavy ions is inertial confinement fusion (ICF) in the so-called ion fast ignition (IFI) option (e.g., [120–128]). In this option, nuclear fuel (e.g., DT) compressed to high densities by many multi-ns laser

beams or X-rays is ignited by the interaction of a very intense picosecond ion beam with the fuel. Compared to the traditional ICF option, in which fuel ignition is a result of its temperature increase accompanying fuel compression, IFI enables fuel ignition and high energy gain of the fusion system with reduced requirements for the compressed fuel and lower total energy of laser drivers. The ion beam parameters required for fuel ignition are, however, extremely high (see sub-sec. 4.2) and at least some of them (beam intensity ~ 10^{20} W/cm^2, ps ion pulse duration) are beyond the capabilities of conventional accelerators. Laser-driven ion accelerators offer the chance to achieve these parameters.

For fuel ignition in the IFI option, both light ions, including protons, and heavy ions can be used. Heavy ion beams have several advantages over light ion beams, particularly the following, (e.g., [66]): (i) The number of ions required for ignition is much smaller than for light ions. (ii) The required ion beam intensities and fluences can be potentially achieved without focusing the beam in the fuel. (iii) Heavy ion beams enable higher energy densities to be deposited in the fuel. (iv) They are less sensitive to (parasitic) electric and magnetic fields occurring in the environment of the compressed fuel. On the other hand, achieving the beam parameters desired for fuel ignition requires significantly higher laser intensities for heavy ions than for light ions. This is primarily due to the fact that the ion energies that ensure efficient deposition of the ion beam energy in the fuel increase with the increase in the ion mass.

The ion energies required for IFI in the case of heavy ions with relatively low mass numbers A ~ 50–100 are of the order of 5–10 GeV; therefore, they are achievable with laser driver parameters similar to those predicted for already constructed multi-PW lasers such as ELI-NP. These lasers are also capable of generating ion beams with ps durations. Therefore, some issues related to IFI can be experimentally studied in the coming years using existing or emerging ultrafast high-peak-power lasers. However, full-scale ICF research in the IFI scenario using heavy ion beams with parameters enabling the ignition of nuclear fuel requires, according to current knowledge, picosecond lasers with energies of ~100–300 kJ (see Section 4.2), i.e., with energies 2–3 orders of magnitude higher than the energies of ultrafast lasers operating today. The prospect of building such lasers is difficult to determine at present, because it depends not only on technological capabilities but also on political decisions. Regardless of this, it can be assumed that the expanding range of other applications of laser-generated heavy ion beams and the increase in power and energy of next-generation ultrafast lasers will stimulate the continuous development of research on the use of these beams in ICF

6.4. Materials Science and Technology

Laser-driven heavy ions can also find applications in some areas of materials science. One of them is the implantation of ions in near-surface layers of various materials (e.g., [145–150]) in order to modify and/or improve the properties of these layers. The main advantage of laser ion sources for implantation over traditional sources (e.g., small conventional accelerators) is the ability to produce ions of virtually any element, as well as the ease of changing one type of ion for another (simply by changing the target). The ion energies required in this application depend on the type of material being implanted and the thickness of the layer in which the ions are to be implanted. Usually, the required energies are not very high and range widely, from several tens of keV to several tens of MeV. Such heavy ion energies are achievable using long-pulse lasers. Energies below 1 MeV can be obtained using commercial lasers with energy $\leq$ 1 J, which can operate with a high repetition rate (~10 Hz or higher) [7] Multi-MeV heavy ion energies require much higher energies of long-pulse lasers, usually ~10–100 J, which most often operate with a very low repetition rate (<<1 Hz) [8,9]. Another parameter of the ion beam that

determines its usefulness in ion implantation is the number of ions in the beam. Long-pulse lasers usually produce a much larger number of ions than ultrafast lasers with similar laser energy, which is, on the one hand, a result of the larger volume of plasma generated by the former (due to their much larger laser focal spot size on the target), and on the other hand, a longer time of ion production in one shot (longer laser–target interaction time). For this reason, in the case of implantation of ions with low energies (several dozen—several hundred keV), long-pulse lasers are much more efficient than ultrafast ones, especially since such ion energies can be achieved using relatively cheap commercial nanosecond lasers operating with a high repetition rate. However, when it comes to implantation of heavy ions with energies of ~multi-MeV, the production of which by long-pulse lasers requires high laser energies that make it impossible to work with a high repetition rate, ultrafast lasers can be more efficient for ion implantation than the long-pulse ones. This is primarily due to the fact that such heavy ion energies can be achieved using ultrafast laser drivers with relatively low energies (~1–10 J), which allow them to work with a high repetition rate. For this reason, the total number of ions implanted in the material per unit time can be orders of magnitude higher than in the case of using a long-pulse laser driver for implantation. However, the use of ultrafast lasers operating at a high repetition rate for heavy ion implantation involves the need to overcome additional challenges.

To produce a beam of heavy ions with a mean energy of ~1 MeV, the intensity of a femtosecond laser pulse at the target should be $\geq 10^{19}$ W/cm^2. This means that for a 100-fs pulse, the laser energy fluence is $\geq$MJ/cm^2, at which a micrometre target is destroyed in no more than a few dozen ns. For repeatable ion generation, a fresh target is necessary after each laser shot. The design of targets that meet this condition is known [68]. It can be, for example, a thin metal tape moving in the focus of the laser beam at a speed adjusted to the laser repetition rate. Therefore, by using a target with a design appropriately matched to the laser parameters, one can avoid heat accumulation in the target and other "parasitic" effects when generating ions with a high repetition rate.

Another issue that needs to be investigated is the possibility of accumulation of "parasitic" effects in the implanted material when illuminating it with an ion beam with a high repetition rate. As already mentioned, the laser beam parameters required for the production of MeV heavy ions can be achieved using a femtosecond laser with an energy of ~1–10 J (peak pulse power in the range of 10–100 TW). Both the repetition rate of such a laser and the target "refresh" rate (e.g., tape speed) are technically and economically limited and are usually in the multi-Hz not multi-kHz range (as in the case of low-energy fs lasers used, e.g., in materials processing [151–153]). In one shot, such a laser can produce ~10^{10}–10^{11} ions with a mean energy of ~1 MeV, which corresponds to an ion beam energy of ~1–10 mJ. If the beam illuminates the surface of the implanted material of ~0.1 cm^2 with a frequency of 10 Hz, the average beam intensity on this surface is ~0.1–1 W/cm^2. Assuming that the ions penetrate the material to a depth of ~1 μm [147], the power density deposited by the ion beam in the material is ~1–10 kW/cm^3. Heat accumulation in the material can therefore be noticeable, although much smaller than under typical conditions of material processing with multi-kHz low-energy fs lasers [151,152]. The power density deposited by the ion beam in the material depends on the type and energy of the ions and the properties of the material. It can be controlled, in particular, by the laser repetition rate and the size of the surface illuminated by the ion beam.

In order for a laser source of heavy ions driven by an ultrafast laser to become practically useful and competitive with traditional sources, significant effort is needed towards (at least) the following: improving the spatial homogeneity of the ion beam, minimising the beam angular divergence, controlling the energy spectrum of the ions, increasing the repetition rate, ensuring a small scatter, and the stability of the beam parameters.

Laser-driven heavy ion beams can also be useful in other areas of materials science. In particular, they can advance research on the behaviour of materials under extreme pressure and/or temperature generated in the material by an ion beam, the study of phase transitions in the material, and others.

7. Summary and Conclusions

Laser-driven ion acceleration is a new, rapidly developing field of research and one of the important applications of ultrafast high-peak-power lasers and laser-produced plasma. In this acceleration method, strong electric fields with strengths reaching tens and hundreds of GV/cm, induced by an ultrafast laser in the plasma generated by the laser–target interaction, enable the acceleration of ions to relativistic velocities on picosecond time scales and at sub-millimetre distances. Using this method, both light and heavy ions can be accelerated, but the latter require much higher laser intensities due to their higher mass, as well as other properties different from those of light ions. For this reason, the development of research on laser-driven heavy ion acceleration and the achieved parameters of heavy ion beams are strongly coupled with the development of ultrafast high-peak-power lasers, primarily with the increase in their peak power and laser beam intensity. The increase in the peak power of ultrafast lasers from the TW level to the PW level observed in the last two decades and the accompanying increase in laser intensity by several orders of magnitude, up to the level of 10^{22} W/cm^2, resulted in the increase in the energy of accelerated heavy ions from ~1 MeV to ~1 GeV, as well as a significant increase in other ion beam parameters such as beam intensity and fluence or the number of generated multi-charge high-energy ions. Further increase in ion beam parameters, including the increase in ion energy to multi-GeV level is possible using currently operating multi-PW lasers, such as ultrafast ELI lasers, provided that the intensity of the generated laser beams increases to ~10^{23} W/cm^2. The production of heavy ion beams with ion energies of tens and hundreds of GeV, i.e., energies comparable to those achieved in large heavy ion accelerators, requires next-generation ultrafast laser drivers (currently designed) with peak power ~100 PW and laser intensity reaching 10^{24} W/cm^2.

Laser-driven heavy ion beams—especially those produced at ultra-high laser intensities (~10^{23} W/cm^2 or higher)—have a number of unique properties unattainable for beams produced in conventional RF-driven accelerators. These include extremely high beam intensities, densities and fluences and very short, pico- or sub-picosecond ion pulse durations. This creates the prospect of using these beams to explore new areas of research in nuclear and particle physics and high energy-density physics, as well as in other fields of research, e.g., inertial confinement fusion. However, many challenges must be overcome to make this prospect a reality. These include the following: (1) Increase in ion energy to sub-TeV and possibly TeV levels (important primarily for applications in nuclear and particle physics). (2) Energy-efficient control of the ion energy spectrum and its narrowing. (3) Control of the beam ionisation spectrum, enabling the generation of mono-charge beams for a wide range of ion mass numbers. (4) Minimisation of the ion beam angular divergence. (5) Increase in the energy efficiency of the generation of high-quality (mono-charge, quasi-monoenergetic, low-divergence) ion beams.

To overcome these challenges, further intensive development of experimental, theoretical, and numerical studies of laser-driven heavy ion acceleration is necessary, especially in the range of ultra-high laser intensities ~10^{23}–10^{24} W/cm^2, which seem to be possible to achieve with the next generation of ultrafast high-peak-power lasers.

Author Contributions: Conceptualisation (lead); formal analysis (equal); writing—original draft (lead), J.B.; formal analysis (equal); software (lead); visualisation (lead), J.D. All authors have read and agreed to the published version of the manuscript.

Funding: This work has been carried out, in part, within the framework of the EUROfusion Consortium, funded by the European Union via the Euratom Research and Training Programme (Grant Agreement No. 101052200—EUROfusion). Views and opinions expressed are, however, those of the authors only and do not necessarily reflect those of the European Union or the European Commission. This scientific work was also supported by the Polish Ministry of Science and Higher Education within the program called "PMW" for 2022 under Contract No. 5246/HEU-Euratom/2022/2. The simulations were carried out with the support of the Interdisciplinary Centre for Mathematical and Computational Modelling (ICM), University of Warsaw under Grant No. G83-16, and the Poznan Supercomputing and Networking Centre under Grant No. 417 and pl0111-01.

Data Availability Statement: The data supporting the findings of the study are available from the corresponding author upon reasonable request.

Conflicts of Interest: The authors have no conflicts of interest to disclose.

References

1. Daido, H.; Nishiuchi, M.; Pirozhkov, A.S. Review of laser driven ion sources and their applications. *Rep. Prog. Phys.* **2012**, *75*, 056401. [CrossRef] [PubMed]
2. Macchi, A.; Borghesi, M.; Passoni, M. Ion acceleration by superintense laser-plasma interaction. *Rev. Mod. Phys.* **2013**, *85*, 751. [CrossRef]
3. Qiao, B.; Shen, X.F.; He, H.; Xie, Y.; Zhang, H.; Zhou, C.T.; Zhu, S.P.; He, X.T. Revisit on ion acceleration mechanisms in solid targets driven by intense laser pulses. *Plasma Phys. Control. Fusion* **2019**, *61*, 014039. [CrossRef]
4. Badziak, J. Laser-driven ion acceleration: Methods, challenges and prospects. *J. Phys. Conf. Series* **2018**, *959*, 012001. [CrossRef]
5. Badziak, J.; Domanski, J. Towards ultra-intense ultra-short ion beams driven by a multi-PW laser. *Laser Part. Beams* **2019**, *37*, 288. [CrossRef]
6. Linlor, W.I. Ion energies produced by laser giant pulse. *Appl. Phys. Lett.* **1963**, *3*, 210–212. [CrossRef]
7. Badziak, J. Laser-driven generation of fast particles. *Opto-Electron. Rev.* **2007**, *15*, 1. [CrossRef]
8. Laska, L.; Jungwirth, K.; Kralikova, B.; Krasa, J.; Pfeifer, M.; Rohlena, K.; Skala, J.; Ullschmied, J.; Badziak, J.; Parys, P.; et al. Generation of multiply charged ions at low and high laser-power densities. *Plasma Phys. Control. Fusion* **2003**, *45*, 585. [CrossRef]
9. Laska, L.; Jungwirth, K.; Krasa, J.; Krousky, E.; Pfeifer, M.; Rohlena, K.; Velyhan, A.; Ullschmied, J.; Gammino, S.; Torrisi, L.; et al. Angular distributions of ions emitted from laser plasma produced at various irradiation angles and laser intensities. *Laser Part. Beams* **2008**, *26*, 555–565. [CrossRef]
10. Danson, C.N.; Haefner, C.; Bromage, J.; Butcher, T.; Chanteloup, J.-C.F.; Chowdhury, E.A.; Galvanauskas, A.; Gizzi, L.A.; Hein, J.; Hillier, D.I.; et al. Petawatt and exawatt class lasers worldwide. *High Power Laser Sci. Eng.* **2019**, *7*, e54. [CrossRef]
11. Radier, C.; Chalus, O.; Charbonneau, M.; Thambirajah, S.; Deschamps, G.; David, S.; Barbe, J.; Etter, E.; Matras, G.; Ricaud, S.; et al. 10 PW peak power femtosecond laser pulse at ELI-NP. *High Power Laser Sci. Eng.* **2022**, *10*, e21. [CrossRef]
12. Wang, P.; Gong, Z.; Lee, S.G.; Shou, Y.; Geng, Y.; Jeon, C.; Kim, I.J.; Lee, H.W.; Yoon, J.W.; Sung, J.H.; et al. Super-Heavy Ions Acceleration Driven by Ultrashort Laser Pulses at Ultrahigh Intensity. *Phys. Rev. X* **2021**, *11*, 021049. [CrossRef]
13. Yoon, J.W.; Kim, Y.G.; Choi, I.W.; Sung, J.H.; Lee, H.W.; Lee, S.K.; Nam, C.H. Realization of laser intensity over 10^{23} W/cm^2. *Optica* **2021**, *8*, 630. [CrossRef]
14. Mourou, G. Nobel Lecture: Extreme light physics and application. *Rev. Mod. Phys.* **2019**, *91*, 030501. [CrossRef]
15. Khazanov, E.; Shaykin, A.; Kostyukov, I.; Ginzburg, V.; Mukhin, I.; Yakovlev, I.; Soloviev, A.; Kuznetsov, I.; Mironov, S.; Korzhimanov, A.; et al. Exawatt Center for Extreme Light Studies (XCELS). *High Power Laser Sci. Eng.* **2023**, *11*, e78. [CrossRef]
16. Wang, X.; Liu, X.; Lu, X.; Chen, J.; Long, Y.; Li, W.; Chen, H.; Chen, X.; Bai, P.; Li, Y.; et al. 13.4fs, 0.1 Hz OPCPA Front End for the 100PW-Class Laser Facility. *Ultrafast Sci.* **2022**, *2022*, 9894358. [CrossRef]
17. Karasik, M.; Weaver, J.L.; Aglitskiy, Y.; Watari, T.; Arikawa, Y.; Sakaiya, T.; Oh, J.; Velikovich, A.L.; Zalesak, S.T.; Bates, J.W.; et al. Acceleration to high velocities and heating by impact using Nike KrF laser. *Phys. Plasmas* **2010**, *17*, 056317. [CrossRef]
18. Badziak, J.; Borodziuk, S.; Pisarczyk, T.; Chodukowski, T.; Krousky, E.; Masek, K.; Skala, J.; Ullschmied, J.; Rhee, Y.-J. Highly efficient acceleration and collimation of high-density plasma using laser-induced cavity pressure. *Appl. Phys. Lett.* **2010**, *96*, 251502. [CrossRef]
19. Badziak, J.; Jabłoński, S.; Pisarczyk, T.; Rączka, P.; Krousky, E.; Liska, R.; Kucharik, M.; Chodukowski, T.; Kalinowska, Z.; Parys, P.; et al. Highly efficient accelerator of dense matter using laser-induced cavity pressure acceleration. *Phys. Plasmas* **2012**, *19*, 053105. [CrossRef]
20. Shui, M.; Chu, G.; Zhu, B.; He, W.; Xi, T.; Fan, W.; Xin, J.; Gu, Y. Hypervelocity launching of flyers at the SG-III prototype laser facility. *J. Appl. Phys.* **2016**, *119*, 035903. [CrossRef]

21. Obenschain, S.P.; Whitlock, R.R.; McLean, E.A.; Ripin, B.H.; Price, R.H.; Phillion, D.W.; Campbell, E.M.; Rosen, M.D.; Auerbach, J.M. Uniform Ablative Acceleration of Targets by Laser Irradiation at 10^{14} W/cm^2. *Phys. Rev. Lett.* **1983**, *50*, 44. [CrossRef]
22. Shui, M.; Chu, G.-B.; Xin, J.-T.; Wu, Y.-C.; Zhu, B.; He, W.-H.; Xi, T.; Gu, Y.-Q. Laser-driven flier impact experiments at the SG-III prototype laser facility. *Chin. Phys. B* **2015**, *24*, 094701. [CrossRef]
23. Atzeni, S.; Meyer-ter-Vehn, J. *The Physics of Inertial Fusion*; Clarendon: Oxford, UK, 2004.
24. Betti, R.; Hurricane, O.A. Inertial-confinement fusion with lasers. *Nat. Phys.* **2016**, *12*, 435. [CrossRef]
25. Hurricane, O.A.; Patel, P.K.; Betti, R.; Froula, D.H.; Regan, S.P.; Slutz, S.A.; Gomez, M.R.; Sweeney, M.A. Physics principles of inertial confinement fusion and U.S. program overview. *Rev. Mod. Phys.* **2023**, *95*, 025005. [CrossRef]
26. Wilks, S.C.; Langdon, A.B.; Cowan, T.E.; Roth, M.; Singh, M.; Hatchett, S.; Key, M.H.; Pennington, D.; McKinnon, A.; Snavely, R.A. Energetic proton generation in ultra-intense laser-solid interactions. *Phys. Plasmas* **2001**, *8*, 542. [CrossRef]
27. Mackinnon, A.J.; Borghesi, M.; Hatchett, S.; Key, M.H.; Patel, P.K.; Campbell, H.; Schiavi, A.; Snavely, R.; Wilks, S.C.; Willi, O. Effect of Plasma Scale Length on Multi-MeV Proton Production by Intense Laser Pulse. *Phys. Rev. Lett.* **2001**, *86*, 1769. [CrossRef] [PubMed]
28. Badziak, J.; Woryna, E.; Parys, P.; Platonov, K.Y.; Jabłoński, S.; Ryć, L.; Vankov, A.B.; Wołowski, J. Fast Proton Generation from Ultrashort Laser Pulse Interaction with Double-Layer Foil Targets. *Phys. Rev. Lett.* **2001**, *87*, 215001. [CrossRef]
29. Mackinnon, A.J.; Sentoku, Y.; Patel, P.K.; Price, D.W.; Hatchett, S.; Key, M.H.; Andersen, C.; Snavely, R.; Freeman, R.R. Enhancement of Proton Acceleration by Hot-Electron Recirculation in Thin Foils Irradiated by Ultraintense Laser Pulses. *Phys. Rev. Lett.* **2002**, *88*, 215006. [CrossRef] [PubMed]
30. Borghesi, M.; Mackinnon, A.J.; Campbell, D.H.; Hicks, D.G.; Kar, S.; Patel, P.K.; Price, D.; Romagnani, L.; Schiavi, A.; Willi, O. Multi-MeV Proton Source Investigations in Ultraintense Laser-Foil Interactions. *Phys. Rev. Lett.* **2004**, *92*, 055003. [CrossRef]
31. Cowan, T.E.; Fuchs, J.; Ruhl, H.; Kemp, A.; Audebert, P.; Roth, M.; Stephens, R.; Barton, I.; Blazevic, A.; Brambrink, E.; et al. Ultralow Emittance, Multi-MeV Proton Beams from a Laser Virtual-Cathode Plasma Accelerator. *Phys. Rev. Lett.* **2004**, *92*, 204801. [CrossRef] [PubMed]
32. Allen, M.; Patel, P.K.; Mackinnon, A.; Price, D.; Wilks, S.; Morse, E. Direct Experimental Evidence of Back-Surface Ion Acceleration from Laser-Irradiated Gold Foils. *Phys. Rev. Lett.* **2004**, *93*, 265004. [CrossRef] [PubMed]
33. Zou, D.B.; Zhuo, H.B.; Yang, X.H.; Yu, T.P.; Shao, F.Q.; Pukhov, A. Control of target-normal-sheath-accelerated protons from a guiding cone. *Phys. Plasmas* **2015**, *22*, 063103. [CrossRef]
34. Zou, D.B.; Yu, D.Y.; Jiang, X.R.; Yu, M.Y.; Chen, Z.Y.; Deng, Z.G.; Yu, T.P.; Yin, Y.; Shao, F.Q.; Zhuo, H.B.; et al. Enhancement of target normal sheath acceleration in laser multi-channel target interaction. *Phys. Plasmas* **2019**, *26*, 123105. [CrossRef]
35. Khan, I.; Saxena, V. Enhanced target normal sheath acceleration with a grooved hydrocarbon target. *Phys. Plasmas* **2023**, *30*, 063102. [CrossRef]
36. Esirkepov, T.; Borghesi, M.; Bulanov, S.V.; Mourou, G.; Tajima, T. Highly Efficient Relativistic-Ion Generation in the Laser-Piston Regime. *Phys. Rev. Lett.* **2004**, *92*, 175003. [CrossRef]
37. Macchi, A.; Cattani, F.; Liseykina, T.V.; Cornalti, F. Laser Acceleration of Ion Bunches at the Front Surface of Overdense Plasmas. *Phys. Rev. Lett.* **2005**, *94*, 165003. [CrossRef] [PubMed]
38. Robinson, A.P.L.; Zepf, M.; Kar, S.; Evans, R.G.; Bellei, C. Radiation pressure acceleration of thin foils with circularly polarized laser pulses. *New J. Phys.* **2008**, *10*, 013021. [CrossRef]
39. Liseykina, T.V.; Borghesi, M.; Macchi, A.; Tuveri, S. Radiation pressure acceleration by ultraintense laser pulses. *Plasma Phys. Control. Fusion* **2008**, *50*, 124033. [CrossRef]
40. Klimo, O.; Psikal, J.; Limpouch, J.; Tikhonchuk, V.T. Monoenergetic ion beams from ultrathin foils irradiated by ultrahigh-contrast circularly polarized laser pulses. *Phys. Rev. ST Accel. Beams* **2008**, *11*, 031301. [CrossRef]
41. Grech, M.; Skupin, S.; Diaw, A.; Schlegel, T.; Tikhonchuk, V.T. Energy dispersion in radiation pressure accelerated ion beams. *New J. Phys.* **2011**, *13*, 123003. [CrossRef]
42. Sgattoni, A.; Sinigardi, S.; Macchi, A. High energy gain in three-dimensional simulations of light sail acceleration. *Appl. Phys. Lett.* **2014**, *105*, 084105. [CrossRef]
43. Zou, D.B.; Zhuo, H.B.; Yu, T.P.; Wu, H.C.; Yang, X.H.; Shao, F.Q.; Ma, Y.Y.; Yin, Y.; Ge, Z.Y. Enhanced laser-radiation-pressure-driven proton acceleration by moving focusing electric-fields in a foil-in-cone target. *Phys. Plasmas* **2015**, *22*, 023109. [CrossRef]
44. Kim, I.J.; Pae, K.H.; Choi, I.W.; Lee, C.-L.; Kim, H.T.; Singhal, H.; Sung, J.H.; Lee, S.K.; Lee, H.W.; Nickles, P.V.; et al. Radiation pressure acceleration of protons to 93 MeV with circularly polarized petawatt laser pulses. *Phys. Plasmas* **2016**, *23*, 070701. [CrossRef]
45. Xu, Y.; Wang, J.; Qi, X.; Li, M.; Xing, Y.; Yang, L.; Zhu, W. Plasma block acceleration via double targets driven by an ultraintense circularly polarized laser pulse. *Phys. Plasmas* **2017**, *24*, 033108. [CrossRef]
46. Badziak, J.; Głowacz, S.; Jabłoński, S.; Parys, P.; Wołowski, J.; Hora, H. Generation of picosecond high-density ion fluxes by skin-layer laser-plasma interaction. *Laser Part. Beams* **2005**, *23*, 143. [CrossRef]

47. Głowacz, S.; Hora, H.; Badziak, J.; Jabłoński, S.; Cang, Y.; Osman, F. Analytical description of rippling effect and ion acceleration in plasma produced by a short laser pulse. *Laser. Part. Beams* **2006**, *24*, 15–25. [CrossRef]
48. Badziak, J.; Jabłoński, S.; Parys, P.; Rosiński, M.; Wołowski, J.; Szydłowski, A.; Antici, P.; Fuchs, J.; Mancic, A. Ultraintense proton beams from laser-induced skin-layer ponderomotive acceleration. *J. Appl. Phys.* **2008**, *104*, 063310. [CrossRef]
49. Silva, L.O.; Marti, M.; Davies, J.R.; Fonseca, R.A. Proton shock acceleration in laser-plasma interactions. *Phys. Rev. Lett.* **2004**, *92*, 015002. [CrossRef]
50. Wei, M.S.; Mangles, S.P.D.; Najmudin, Z.; Walton, B.; Gopal, A.; Tatarakis, M.; Dangor, A.E.; Clark, E.L.; Evans, R.G.; Fritzler, S.; et al. Ion acceleration by collisionless shocks in high-intensity-laser–underdense-plasma interaction. *Phys. Rev. Lett.* **2004**, *93*, 155003. [CrossRef]
51. Esirkepov, T.; Bingham, R.; Bulanov, S.; Honda, T.; Nishihara, K.; Pegoraro, F. Coulomb explosion of a cluster irradiated by a high intensity laser pulse. *Laser Part. Beams* **2000**, *18*, 503. [CrossRef]
52. Bychenkov, V.Y.; Kovaliev, V.F. Coulomb explosion in a cluster plasma. *Plasma Phys. Rep.* **2005**, *31*, 178–183. [CrossRef]
53. Sarkisov, G.S.; Bychenkov, V.Y.; Novikov, V.N.; Tikhonchuk, V.T.; Maksimchuk, A.; Chen, S.-Y.; Wagner, R.; Mourou, G.; Umstandter, D. Self-focusing, channel formation, and high-energy ion generation in interaction of an intense short laser pulse with a He jet. *Phys. Rev. E* **1999**, *59*, 7042. [CrossRef]
54. Stoian, R.; Ashkenasi, D.; Rosenfeld, A.; Campbell, E.E.B. Coulomb explosion in ultrashort pulsed laser ablation of Al_2O_3. *Phys. Rev. B* **2000**, *62*, 13167. [CrossRef]
55. Bychenkov, V.Y.; Brantov, A.V.; Govras, E.A.; Kovalev, V.F. Laser acceleration of ions: Recent results and prospects for applications. *Physics-Uspekhi* **2015**, *58*, 71B. [CrossRef]
56. Yin, L.; Albright, B.J.; Hegelich, B.M.; Fernandez, J.C. GeV laser ion acceleration from ultrathin targets: The laser breakout afterburner. *Laser Part. Beams* **2006**, *24*, 291–298. [CrossRef]
57. Yin, L.; Albright, B.J.; Hegelich, B.M.; Browers, K.J.; Flippo, K.A.; Kwan, T.J.T.; Fernandez, J.C. Monoenergetic and GeV ion acceleration from the laser breakout afterburner using ultrathin targets. *Phys. Plasmas* **2007**, *14*, 056706. [CrossRef]
58. Hegelich, B.M.; Pomerantz, I.; Yin, L.; Wu, H.C.; Jung, D.; Albright, B.J.; Gautier, D.C.; Letzring, S.; Palaniyappan, S.; Shah, R.; et al. Laser-driven ion acceleration from relativistically transparent nanotargets. *New J. Phys.* **2013**, *15*, 085015. [CrossRef]
59. Higginson, A.; Gray, R.J.; King, M.; Dance, R.J.; Williamson, S.D.R.; Butler, N.M.H.; Wilson, R.; Capdessus, R.; Armstrong, C.; Green, J.S.; et al. Near-100 MeV protons via a laser-driven transparency-enhanced hybrid acceleration scheme. *Nat. Commun.* **2018**, *9*, 724. [CrossRef] [PubMed]
60. Nakamura, T.; Bulanov, S.V.; Esirkepov, T.Z.; Kando, M. High-Energy Ions from Near-Critical Density Plasmas via Magnetic Vortex Acceleration. *Phys. Rev. Lett.* **2010**, *105*, 135002. [CrossRef]
61. Park, J.; Bulanov, S.S.; Bin, J.; Ji, Q.; Steinke, S.; Vay, J.-L.; Geddes, C.G.R.; Schroeder, C.B.; Leemans, W.P.; Schenkel, T.; et al. Ion acceleration in laser generated megatesla magnetic vortex. *Phys. Plasmas* **2019**, *26*, 103108. [CrossRef]
62. Jung, D.; Yin, L.; Albright, B.J.; Gautier, D.C.; Hörlein, R.; Kiefer, D.; Henig, A.; Johnson, R.; Letzring, S.; Palaniyappan, S.; et al. Monoenergetic Ion Beam Generation by Driving Ion Solitary Waves with Circularly Polarized Laser Light. *Phys. Rev. Lett.* **2011**, *107*, 115002. [CrossRef] [PubMed]
63. Yin, L.; Albright, B.J.; Jung, D.; Bowers, K.J.; Shah, R.C.; Palaniyappan, S.; Fernández, J.C.; Hegelich, B.M. Mono-energetic ion beam acceleration in solitary waves during relativistic transparency using high-contrast circularly polarized short-pulse laser and nanoscale targets. *Phys. Plasmas* **2011**, *18*, 053103. [CrossRef]
64. Domański, J.; Badziak, J. Towards single-charge heavy ion beams driven by an ultra-intense laser. *Plasma Phys. Control. Fusion* **2022**, *64*, 085002. [CrossRef]
65. Domański, J.; Badziak, J. Super-heavy ion beams generated by a multi-PW femtosecond laser. *Phys. Plasmas* **2024**, *31*, 023110. [CrossRef]
66. Badziak, J.; Domański, J. In search of ways to improve the properties of a laser-accelerated heavy ion beam relevant for fusion fast ignition. *Phys. Plasmas* **2023**, *30*, 053107. [CrossRef]
67. Hora, H. *Physics of Laser Driven Plasmas*; Wiley: New York, USA, 1981.
68. Eliezer, S.; Nissim, N.; Martinez Val, J.M.; Mima, K.; Hora, H. Double layer acceleration by laser radiation. *Laser Part. Beams* **2014**, *32*, 211. [CrossRef]
69. Petrov, G.M.; McGuffey, C.; Thomas, A.G.R.; Krushelnick, K.; Beg, F.N. Generation of heavy ion beams using femtosecond laser pulses in the target normal sheath acceleration and radiation pressure acceleration regimes. *Phys. Plasmas* **2016**, *23*, 063108. [CrossRef]
70. Roth, M.; Blazevic, A.; Geissel, M.; Schlegel, T.; Cowan, T.E.; Allen, M.; Gauthier, J.-C.; Audebert, P.; Fuchs, J.; Meyer-ter-Vehn, J.; et al. Energetic ions generated by laser pulses: A detailed study on target properties. *Phys. Rev. ST Accel. Beams* **2002**, *5*, 0613001. [CrossRef]

71. Snavely, R.A.; Key, M.H.; Hatchett, S.P.; Cowan, T.E.; Roth, M.; Philips, T.W.; Stoyer, M.A.; Henry, E.A.; Sangster, T.C.; Singh, M.S.; et al. Intense High-Energy Proton Beams from Petawatt-Laser Irradiation of Solids. *Phys. Rev. Lett.* **2000**, *85*, 2945. [CrossRef] [PubMed]
72. Brenner, C.M.; Robinson, A.P.L.; Markey, K.; Scott, R.H.H.; Gray, R.J.; Rosiński, M.; Deppert, O.; Badziak, J.; Batani, D.; Davies, J.R.; et al. High energy conversion efficiency in laser-proton acceleration by controlling laser-energy deposition onto thin foil targets. *Appl. Phys. Lett.* **2014**, *104*, 081123. [CrossRef]
73. Petrov, M.; Willingale, L.; Davis, J.; Petrova, T.; Maksimchuk, A.; Krushelnick, K. The impact of contaminants on laser-driven light ion acceleration. *Phys. Plasmas* **2010**, *17*, 103111. [CrossRef]
74. Domański, J.; Badziak, J. Properties of heavy ion beams produced by a PW sub-picosecond laser. *J. Instrum.* **2020**, *15*, C05037. [CrossRef]
75. Petrov, G.M.; McGuffey, C.; Thomas, A.G.R.; Krushelnick, K.; Beg, F.N. Heavy ion acceleration in the radiation pressure acceleration and breakout afterburner regimes. *Plasma Phys. Control. Fusion* **2017**, *59*, 075003. [CrossRef]
76. Badziak, J.; Jabłoński, S. Acceleration of a solid-density plasma projectile to ultrahigh velocities by a short-pulse ultraviolet laser. *Appl. Phys. Lett.* **2010**, *99*, 071502. [CrossRef]
77. Palmer, C.A.J.; Schreiber, J.; Nagel, S.R.; Dover, N.P.; Bellei, C.; Beg, F.N.; Bott, S.; Clarke, R.J.; Dangor, A.E.; Hassan, S.M.; et al. Rayleigh-Taylor Instability of an Ultrathin Foil Accelerated by the Radiation Pressure of an Intense Laser. *Phys. Rev. Lett.* **2012**, *108*, 225002. [CrossRef]
78. Sgattoni, A.; Sinigardi, S.; Fedeli, L.; Pegoraro, F.; Macchi, A. Laser-driven Rayleigh-Taylor instability: Plasmonic effects and three-dimensional structures. *Phys. Rev. E* **2015**, *91*, 013106. [CrossRef] [PubMed]
79. Laska, L.; Badziak, J.; Gammino, S.; Jungwirth, K.; Kasperczuk, A.; Krasa, J.; Krousky, E.; Kubes, P.; Parys, P.; Pfeifer, M.; et al. The influence of an intense laser beam interaction with preformed plasma on the characteristics of emitted ion streams. *Laser Part. Beams* **2007**, *25*, 549. [CrossRef]
80. Torrisi, L.; Cutroneo, M.; Andò, L.; Ullschmied, J. Thomson parabola spectrometry for gold laser-generated plasmas. *Phys. Plasmas* **2013**, *20*, 023106. [CrossRef]
81. Badziak, J.; Kasperczuk, A.; Parys, P.; Pisarczyk, T.; Rosiński, M.; Ryć, L.; Wołowski, J.; Jabłoński, S.; Suchańska, R.; Krousky, E.; et al. Production of high-current heavy ion jets at the short-wavelength subnanosecond laser-solid interaction. *Appl. Phys. Lett.* **2007**, *91*, 081502. [CrossRef]
82. Prencipe, I.; Fuchs, J.; Pascarelli, S.; Schumacher, D.W.; Stephens, R.B.; Alexander, N.B.; Briggs, R.; Büscher, M.; Cernaianu, M.O.; Choukourov, A.; et al. Targets for high repetition rate laser facilities: Needs, challenges and perspectives. *High Power Laser Sci. Eng.* **2017**, *5*, e17. [CrossRef]
83. Badziak, J.; Makowski, J.; Parys, P.; Ryć, L.; Wołowski, J.; Woryna, E.; Vankov, A.B. Intensity-dependent characteristics of a picosecond laser-produced Cu plasma. *J. Phys. D Appl. Phys.* **2001**, *34*, 1885. [CrossRef]
84. Badziak, J.; Makowski, J.; Parys, P.; Wołowski, J.; Woryna, E.; Vankov, A.B. Generation of streams of highly charged Ag ions by picosecond laser. *Appl. Phys. Lett.* **2001**, *78*, 1823. [CrossRef]
85. Badziak, J.; Parys, P.; Vankov, A.B.; Wołowski, J.; Woryna, E. Generation of fluxes of highly charged ions from a picosecond laser-produced plasma. *Appl. Phys. Lett.* **2001**, *79*, 21. [CrossRef]
86. Badziak, J.; Hora, H.; Woryna, E.; Jabłoński, S.; Laska, L.; Parys, P.; Rohlena, K.; Wołowski, J. Experimental evidence of differences in properties of fast ion fluxes from short-pulse and long-pulse laser-plasma interactions. *Phys. Lett. A* **2003**, *315*, 452. [CrossRef]
87. Clark, E.L.; Krushelnick, K.; Zepf, M.; Beg, F.N.; Tatarakis, M.; Machacek, A.; Santala, M.I.K.; Watts, I.; Norreys, P.A.; Dangor, A.E. Energetic heavy-ion and proton generation from ultraintense laser-plasma interactions with solids. *Phys. Rev. Lett.* **2000**, *85*, 1654. [CrossRef]
88. McKenna, P.; Ledingham, K.W.D.; Yang, J.M.; Robson, L.; McCanny, T.; Shimizu, S.; Clarke, R.J.; Neely, D.; Spohr, K.; Chapman, R.; et al. Characterization of proton and heavier ion acceleration in ultrahigh-intensity laser interactions with heated target foils. *Phys. Rev. E* **2004**, *70*, 036405. [CrossRef] [PubMed]
89. McKenna, P.; Lindau, F.; Lundh, O.; Carroll, D.C.; Clarke, R.J.; Ledingham, K.W.D.; McCanny, T.; Neely, D.; Robinson, A.P.L.; Robson, L.; et al. Low- and medium-mass ion acceleration driven by petawatt laser plasma interactions. *Plasma Phys. Control. Fusion* **2007**, *49*, B223–B231. [CrossRef]
90. Tayyab, M.; Bagchi, S.; Chakera, J.A.; Avasthi, D.K.; Ramis, R.; Upadhyay, A.; Ramakrishna, B.; Mandal, T.; Naik, P.A. Mono-energetic heavy ion acceleration from laser plasma based composite nano-accelerator. *Phys. Plasmas* **2018**, *25*, 123102. [CrossRef]
91. Bagchi, S.; Tayyab, M.; Pasley, J.; Robinson, A.P.L.; Nayak, M.; Chakera, J.A. Quasi mono-energetic heavy ion acceleration from layered targets. *Phys. Plasmas* **2021**, *28*, 023108. [CrossRef]
92. Nishiuchi, M.; Sakaki, H.; Esirkepov, T.Z.; Nishio, K.; Pikuz, T.A.; Faenov, A.Y.; Skobelev, I.Y.; Orlandi, R.; Sako, H.; Pirozhkov, A.S.; et al. Acceleration of highly charged GeV Fe ions from a low-Z substrate by intense femtosecond laser. *Phys. Plasmas* **2015**, *22*, 033107. [CrossRef]

93. Braenzel, J.; Andreev, A.A.; Platonov, K.; Klingsporn, M.; Ehrentraut, L.; Sandner, W.; Schnurer, M. Coulomb-Driven Energy Boost of Heavy Ions for Laser-Plasma Acceleration. *Phys. Rev. Lett.* **2015**, *114*, 124801. [CrossRef] [PubMed]
94. Lindner, F.H.; McCary, E.; Jiao, X.; Ostermayr, T.M.; Roycroft, R.; Tiwari, G.; Hegelich, B.M.; Schreiber, J.; Thirolf, P.G. En-route to the fission–fusion reaction mechanism: A status update on laser-driven heavy ion acceleration. *Plasma Phys. Control. Fusion* **2019**, *61*, 055002. [CrossRef]
95. Nishiuchi, M.; Dover, N.P.; Hata, M.; Sakaki, H.; Kondo, K.; Lowe, H.F.; Miyahara, T.; Kiriyama, H.; Koga, J.K.; Iwata, N.; et al. Dynamics of laser-driven heavy-ion acceleration clarified by ion charge states. *Phys. Rev. Res.* **2020**, *2*, 033081. [CrossRef]
96. Lindner, F.H.; Fitzpatrick, E.G.; Haffa, D.; Ponnath, L.; Schmidt, A.-K.; Speicher, M.; Zielbauer, B.; Schreiber, J.; Thirolf, P.G. Charge-state resolved laser acceleration of gold ions to beyond 7 MeV/u. *Sci. Rep.* **2022**, *12*, 4784. [CrossRef]
97. Hollinger, R.; Wang, S.; Wang, Y.; Moreau, A.; Capeluto, M.G.; Song, H.; Rockwood, A.; Bayarsaikhan, E.; Kaymak, V.; Pukhov, A.; et al. Extreme ionization of heavy atoms in solid-density plasmas by relativistic second-harmonic laser pulses. *Nat. Photonics* **2020**, *14*, 607. [CrossRef]
98. Doria, D.; Martin, P.; Ahmed, H.; Alejo, A.; Cerchez, M.; Ferguson, S.; Fernandez-Tobias, J.; Green, J.S.; Gwynne, D.; Hanton, F.; et al. Calibration of BAS-TR image plate response to GeV gold ions. *Rev. Sci. Instrum.* **2022**, *93*, 033304. [CrossRef]
99. Martin, P.; Ahmed, H.; Doria, D.; Cerchez, M.; Hanton, F.; Gwynne, D.; Alejo, A.; Fernández-Tobías, J.; Green, J.; Macchi, A.; et al. Narrow-band acceleration of gold ions to GeV energies from ultra-thin foils. *Commun. Phys.* **2024**, *7*, 3. [CrossRef]
100. Korzhimanov, A.V.; Efimenko, E.S.; Golubev, S.V.; Kim, A.V. Generating High-Energy Highly Charged Ion Beams from Petawatt-Class Laser Interactions with Compound Targets. *Phys. Rev. Lett.* **2012**, *109*, 245008. [CrossRef]
101. Wu, D.; Qiao, B.; McGuffey, C.; He, X.T.; Beg, F.N. Generation of high-energy mono-energetic heavy ion beams by radiation pressure acceleration of ultra-intense laser pulses. *Phys. Plasmas* **2014**, *21*, 123118. [CrossRef]
102. Wang, H.Y.; Lin, C.; Liu, B.; Sheng, Z.M.; Lu, H.Y.; Ma, W.J.; Bin, J.H.; Schreiber, J.; He, X.T.; Chen, J.E.; et al. Laser-driven three-stage heavy-ion acceleration from relativistic laser-plasma interaction. *Phys. Rev. E* **2014**, *89*, 013107. [CrossRef]
103. Shen, X.F.; Qiao, B.; Zhang, H.; Kar, S.; Zhou, C.T.; Chang, H.X.; Borghesi, M.; He, X.T. Achieving Stable Radiation Pressure Acceleration of Heavy Ions via Successive Electron Replenishment from Ionization of a High-Z Material Coating. *Phys. Rev. Lett.* **2017**, *118*, 204802. [CrossRef] [PubMed]
104. Li, J.; Arefiev, A.V.; Bulanov, S.S.; Kawahito, D.; Bailly-Grandvaux, M.; Petrov, G.M.; McGuffey, C.; Beg, F.N. Ionization injection of highly-charged copper ions for laser driven acceleration from ultra-thin foils. *Sci. Rep.* **2019**, *9*, 666. [CrossRef]
105. Kawahito, D.; Kishimoto, Y. Ionization and acceleration of multiply charged gold ions in solid film irradiated by high intensity laser. *Phys. Plasmas* **2020**, *27*, 033108. [CrossRef]
106. Afshari, M.; Morris, S.; Geulig, L.D.; Chitgar, Z.M.; Gibbon, P.; Thirolf, P.G.; Schreiber, J. The role of collisional ionization in heavy ion acceleration by high intensity laser pulses. *Sci. Rep.* **2022**, *12*, 18260. [CrossRef]
107. Mehrangiz, M. Application of encapsulated hollow gold nanocluster targets for high-quality and quasi-monoenergetic ions generation. *Plasma Phys. Control. Fusion* **2022**, *64*, 035007. [CrossRef]
108. Wu, D.; Qiao, B.; He, X.T. The radiation reaction effects in the ultra-intense and ultra-short laser foil interaction regime. *Phys. Plasmas* **2015**, *22*, 093108. [CrossRef]
109. Domański, J.; Badziak, J. Ultra-intense femtosecond super-heavy ion beams driven by a multi-PW laser. *Phys. Lett. A* **2018**, *382*, 3412. [CrossRef]
110. Zhao, N.; Zou, D.B.; Jiang, X.R.; Yu, T.P.; Yu, M.Y.; Liu, K.; Huang, T.W.; Zhang, H.; Wu, S.Z.; Hu, L.X.; et al. Hundreds-GeV Au ion generation by $10^{22–24}$ W cm^{-2} laser pulses interacting with high-Z grain doped gas. *Plasma Phys. Control. Fusion* **2021**, *63*, 035009. [CrossRef]
111. Zou, D.; Yu, M.; Jiang, X.; Zhao, N.; Yu, T.; Zhuo, H.; Pukhov, A.; Ma, Y.; Shao, F.; Zhou, C.; et al. Highly Efficient Heavy Ion Acceleration from Laser Interaction with Dusty Plasma. *Adv. Photonics Res.* **2021**, *2*, 2000181. [CrossRef]
112. Zhao, N.; Gan, L.; Liu, K.; Zou, D.; Zhou, Y.; Zhang, G.; Wang, W.; Zhuo, H. Quasi monoenergetic heavy ion acceleration driven by sub-100 PW linearly polarized laser pulses in the radiation-dominated QED regime. *Phys. Plasmas* **2024**, *31*, 033103. [CrossRef]
113. Tamburini, M.; Pegoraro, F.; Di Piazza, A.; Keitel, C.H.; Macchi, A. Radiation reaction effects on radiation pressure acceleration. *New. J. Phys.* **2010**, *12*, 123005. [CrossRef]
114. Ridgers, C.P.; Brady, C.S.; Duclous, R.; Kirk, J.G.; Bennett, K.; Arber, T.D.; Robinson, A.P.L.; Bell, A.R. Dense electron-positron plasmas and ultraintense γ rays from laser-irradiated solids. *Phys. Rev. Lett.* **2012**, *108*, 165006. [CrossRef]
115. Brady, C.S.; Ridges, C.P.; Arber, T.D.; Bell, A.R. Synchrotron radiation, pair production, and longitudinal electron motion during 10-100 PW laser solid interaction. *Phys. Plasmas* **2014**, *21*, 033108. [CrossRef]
116. Capdessus, R.; McKenna, P. Influence of radiation force on ultraintense laser-driven ion acceleration. *Phys. Rev. E* **2015**, *91*, 053105. [CrossRef] [PubMed]
117. Del Sorbo, D.; Blackman, D.R.; Capdessus, R.; Small, K.; Slade-Lowther, C.; Luo, W.; Duff, M.J.; Robinson, A.P.L.; McKenna, P.; Sheng, Z.-M.; et al. Efficient ion acceleration and dense electron–positron plasma creation in ultra-high intensity laser-solid interactions. *New J. Phys.* **2018**, *20*, 033014. [CrossRef]

118. Popruzhenko, S.V.; Liseykina, T.V.; Macchi, A. Efficiency of radiation friction losses in laser-driven 'hole boring' of dense targets. *New J. Phys.* **2019**, *21*, 033009. [CrossRef]
119. Domański, J.; Badziak, J. Generation of ion beams from a high-Z target irradiated by a laser pulse of ultra-relativistic intensity. *Acta Phys. Polon. A* **2020**, *138*, 586. [CrossRef]
120. Tabak, M.; Hammer, J.; Glinsky, M.E.; Kruer, W.L.; Wilks, S.C.; Woodworth, J.; Campbell, E.M.; Perry, M.D.; Mason, R.J. Ignition and high gain with ultrapowerful lasers. *Phys. Plasmas* **1994**, *1*, 1626. [CrossRef]
121. Roth, M.; Cowan, T.E.; Key, M.H.; Hatchett, S.P.; Brown, C.; Fountain, W.; Johnson, J.; Pennington, D.M.; Snavely, R.A.; Wilks, S.C.; et al. Fast ignition by intense laser-accelerated proton beams. *Phys. Rev. Lett.* **2001**, *86*, 436. [CrossRef]
122. Bychenkov, V.Y.; Rozmus, W.; Maksimchuk, A.; Umstadter, D.; Capjack, C.E. Fast Ignitor Concept with Light Ions. *Plasma Phys. Rep.* **2001**, *27*, 1017. [CrossRef]
123. Temporal, M.; Honrubia, J.J.; Atzeni, S. Numerical study of fast ignition of ablatively imploded deuterium-tritium fusion capsules by ultra-intense proton beams. *Phys. Plasmas* **2002**, *9*, 3098. [CrossRef]
124. Key, M.H. Status of and prospects for the fast ignition inertial fusion concept. *Phys. Plasmas* **2007**, *14*, 055502. [CrossRef]
125. Badziak, J.; Jabłoński, S.; Wołowski, J. Progress and prospect of fast ignition of ICF targets. *Plasma Phys. Control. Fusion* **2007**, *49*, B651. [CrossRef]
126. Honrubia, J.J.; Fernandez, J.C.; Temporal, M.; Hegelich, B.M.; Meyer-ter-Vehn, J. Fast ignition of inertial fusion targets by laser-driven carbon beams. *Phys. Plasmas* **2009**, *16*, 102701. [CrossRef]
127. Fernandez, J.C.; Albright, B.J.; Beg, F.N.; Foord, M.E.; Hegelich, B.M.; Honrubia, J.J.; Roth, M.; Stephens, R.B.; Yin, L. Fast ignition with laser-driven proton and ion beams. *Nucl. Fusion* **2014**, *54*, 054006. [CrossRef]
128. Badziak, J.; Domański, J. Laser-driven acceleration of ion beams for high-gain inertial confinement fusion. *Nucl. Fusion* **2021**, *61*, 046011. [CrossRef]
129. Honrubia, J.J.; Fernandez, J.C.; Hegelich, B.M.; Murakami, M.; Enriquez, C.D. Fast ignition driven by quasi-monoenergetic ions: Optimal ion type and reduction of ignition energies with an ion beam array. *Laser Part. Beams* **2014**, *32*, 419. [CrossRef]
130. Honrubia, J.J.; Murakami, M. Ion beam requirements for fast ignition of inertial fusion targets. *Phys. Plasmas* **2015**, *22*, 012703. [CrossRef]
131. Davis, J.; Petrov, G.M.; Mehlhorn, T.A. Generation of laser-driven light ions suitable for fast ignition of fusion targets. *Plasma Phys. Control. Fusion* **2011**, *53*, 045013. [CrossRef]
132. Di Piazza, A.; Müller, C.; Hatsagortsyan, K.Z.; Keitel, C.H. Extremely high-intensity laser interactions with fundamental quantum systems. *Rev. Mod. Phys.* **2012**, *84*, 1177. [CrossRef]
133. Gonoskov, A.; Blackburn, T.G.; Marklund, M.; Bulanov, S.S. Charged particle motion and radiation in strong electromagnetic fields. *Rev. Mod. Phys.* **2022**, *94*, 045001. [CrossRef]
134. Badziak, J.; Domański, J. Laser-driven acceleration of ion beams for ion fast ignition: The effect of the laser wavelength on the ion beam properties. *Plasma Phys. Control. Fusion* **2021**, *63*, 055005. [CrossRef]
135. Badziak, J.; Domański, J. Ultra-intense laser-accelerated ion beams for high-gain inertial fusion: The effect of the ion mass on the beam properties. *Nucl. Fusion* **2022**, *62*, 086040. [CrossRef]
136. Bulanov, S.S.; Esarey, E.; Schroeder, C.B.; Bulanov, S.V.; Esirkepov, T.Z.; Kando, M.; Pegoraro, F.; Leemans, W.P. Radiation pressure acceleration: The factors limiting maximum attainable ion energy. *Phys. Plasmas* **2016**, *23*, 056703. [CrossRef]
137. Jain, S.; Soni, K.K.; Jaiman, N.K.; Maheshwari, K.P. Effect of Laser Group Velocity on Maximum Attainable Ion Energy in the Radiation Pressure Dominant (RPD) Regime. *IEEE Trans. Plasma Sci.* **2021**, *49*, 1253–1258. [CrossRef]
138. Negoita, F.; Roth, M.; Thirolf, P.G.; Tudisco, S.; Hannachi, F.; Moustaizis, S.; Pomerantz, I.; McKenna, P.; Fuchs, J.; Sphor, K.; et al. Laser driven nuclear physics at ELI_NP. *Rom. Rep. Phys.* **2016**, *68*, S37–S144.
139. Gales, S.; Tanaka, K.A.; Balabanski, D.L.; Negoita, F.; Stutman, D.; Tesileanu, O.; Ur, C.A.; Ursescu, D.; Andrei, I.; Ataman, S.; et al. The extreme light infrastructure-nuclear physics (ELI-NP) facility: New horizons in physics with 10 PW ultra-intense lasers and 20 MeV brilliant gamma beams. *Rep. Prog. Phys.* **2018**, *81*, 094301. [CrossRef] [PubMed]
140. Domański, J.; Badziak, J.; Marchwiany, M. Laser-driven acceleration of heavy ions at ultra-relativistic laser intensity. *Laser. Part. Beams* **2018**, *36*, 507. [CrossRef]
141. Sturm, C.; Böttcher, I.; Dębowski, M.; Förster, A.; Grosse, E.; Koczoń, P.; Kohlmeyer, B.; Laue, F.; Mang, M.; Naumann, L.; et al. Evidence for a Soft Nuclear Equation-of-State from Kaon Production in Heavy-Ion Collisions. *Phys. Rev. Lett.* **2001**, *86*, 39. [CrossRef]
142. Drake, R.P. *High-Energy-Density Physics*; Springer: Berlin/Heidelberg, Germany, 2006.
143. Hoffmann, D.H.H.; Fortov, V.E.; Kuster, M.; Mintsev, V.; Sharkov, B.Y.; Tahir, N.A.; Udrea, S.; Varentsov, D.; Weyrich, K. High energy density physics generated by intense heavy ion beams. *Astrophys. Space Sci.* **2009**, *322*, 167. [CrossRef]
144. Sharkov, B.Y.; Hoffmann, D.H.H.; Golubev, A.A.; Zhao, Y. High energy density physics with intense ion beams. *Matter Radiat. Extrem.* **2016**, *1*, 28. [CrossRef]

145. Boody, F.P.; Hopel, R.; Hora, H.; Kelly, J.C. Laser-driven ion source for reduced-cost implantation of metal ions for strong reduction of dry friction and increased durability. *Laser Part. Beams* **1996**, *14*, 443–448. [CrossRef]
146. Torrisi, L.; Gammino, S.; Mezzasalma, A.M.; Badziak, J.; Parys, P.; Wołowski, J.; Woryna, E.; Krasa, J.; Laska, L.; Pfeifer, M.; et al. Implantation of ions produced by the use of high power iodine laser. *Appl. Surf. Sci.* **2003**, *217*, 319–331. [CrossRef]
147. Rosiński, M.; Badziak, J.; Boody, F.P.; Gammino, S.; Hora, H.; Krasa, J.; Laska, L.; Mezzasalma, A.M.; Parys, P.; Rohlena, K.; et al. Application of laser ion source for ion implantation technology. *Vacuum* **2005**, *78*, 435. [CrossRef]
148. Wołowski, J.; Badziak, J.; Czarnecka, A.; Parys, P.; Pisarek, M.; Rosiński, M.; Turan, R.; Yerci, S. Application of pulsed laser deposition and laser-induced ion implantation for formation of semiconductor nano-crystallites. *Laser Part. Beams* **2007**, *25*, 65–69. [CrossRef]
149. Cutroneo, M.; Torrisi, L.; Ullschmied, J.; Dudzak, R. Multi-energy ion implantation from high-intensity laser. *Nukleonika* **2016**, *61*, 109. [CrossRef]
150. Cutroneo, M.; Mackova, A.; Torrisi, L.; Lavrentiev, V. Laser ion implantation of Ge in SiO_2 using a post-ion acceleration system. *Laser Part. Beams* **2017**, *35*, 72–80. [CrossRef]
151. Jia, X.; Chen, Y.; Liu, L.; Wang, C.; Duan, J. Combined pulse laser: Reliable tool for high-quality, high-efficiency material processing. *Opt. Laser Techn.* **2022**, *153*, 108209. [CrossRef]
152. Jia, X.; Luo, J.; Li, K.; Wang, C.; Li, Z.; Wang, M.; Jiang, Z.; Veiko, V.P.; Duan, J. Ultrafast laser welding of transparent materials: From principles to applications. *Int. J. Extrem. Manuf.* **2025**, *7*, 032001. [CrossRef]
153. Li, Z.; Lin, J.; Wang, C.; Li, K.; Jia, X.; Wang, C.; Duan, J. Damage performance of alumina ceramic by femtosecond laser induced air filamentation. *Opt. Laser Techn.* **2022**, *181*, 111781. [CrossRef]

Disclaimer/Publisher's Note: The statements, opinions and data contained in all publications are solely those of the individual author(s) and contributor(s) and not of MDPI and/or the editor(s). MDPI and/or the editor(s) disclaim responsibility for any injury to people or property resulting from any ideas, methods, instructions or products referred to in the content.